RSC Advances

RSC Publishing

REVIEW

Computational simulations of solid state NMR spectra: a new era in structure determination of oxide glasses

Cite this: *RSC Advances*, 2013, **3**, 10550

Thibault Charpentier,†[a] Maria Cristina Menziani†*[b] and Alfonso Pedone†[b]

Received 5th February 2013,
Accepted 14th March 2013

DOI: 10.1039/c3ra40627j

www.rsc.org/advances

The application of the MD–GIPAW approach to the calculation of NMR parameters, line widths and shapes of the spectra of oxide glasses is reviewed. Emphasis is given to the decisive role of this approach both as an interpretative tool for a deeper understanding of the spectral behavior of complex systems and as a predictive instrument to map NMR data in a distribution of structural parameters and *vice versa* (structural inversion method). After a brief overview of the basic features of oxide glasses and the experimental techniques routinely employed to investigate their structure, a general description of the computational methods usually adopted to generate sound structural models of amorphous materials is offered. The computational recipe used to compute the solid state NMR spectra of oxide glasses and to establish quantitative structural-NMR property relationships is then described. Finally, these concepts are applied to 'simple' network former glasses and more complex silicates, aluminosilicate, phosphosilicate and borosilicate glasses of scientific relevance. The final section is dedicated to the future developments that will hopefully improve the computational approach described overcoming some of the current limitations.

1. Introduction

Amorphous inorganic materials are being increasingly used for addressing major technological challenges in energy, medicine and advanced communication systems. Thus, for example, the design of substrate or coating glasses with appropriate characteristics will play an enabling role in the development of roll-to-roll processing of solar cells, encapsulation of organic semiconductors, flexible displays, next-generation touch-screen devices and scaffolds for bone tissue engineering.[1,2]

The crucial issue for the development of such materials is an improved understanding of their fundamental structure–

[a]*CEA, IRAMIS, SIS2M, CEA-CNRS UMR 3299, 91191 Gif-sur-Yvette cedex, France*
[b]*Dipartimento di Scienze Chimiche e Geologiche, Università degli Studi di Modena e Reggio Emilia, Via G. Campi 183, 41125 Modena, Italy. E-mail: menziani@unimo.it; Fax: +39 059 3735; Tel: +39 059 2055091*
† The authors made equal contributions.

Thibault Charpentier†

Thibault Charpentier has been working in CEA Saclay since 1998 when he received his Ph.D. (NMR of quadrupolar nuclei in solids). In 1999 he was awarded the Louis Armand Prize from the French Academy of Science. He obtained his habilitation thesis in 2008. His research interest is theoretical (spin dynamics and quantum mechanics) and computational (DFT–GIPAW calculations and molecular dynamics simulations) NMR. He is also interested in the development and application of NMR to elucidate the structure of glasses and nuclear waste materials. He is the author of more than 75 publications in peer-reviewed international journals.

Maria Cristina Menziani

Maria Cristina Menziani received her Ph.D. in Chemistry from the Università degli Studi of Modena and Reggio Emilia, where she is an Associate Professor in Physical Chemistry and Director of the Doctorate School in "Multiscale Modelling, Computational Simulations and Characterization in Material and Life Sciences". Her research aims to develop computational strategies for rationalizing and interpreting the behaviour of biomolecular systems, inorganic amorphous materials and biomaterials. Many projects are carried out with experimentalists and emphasis is given on material design, lead discovery and theranostic development. She is the author of more than 130 publications in peer-reviewed international journals.

property relationships. Unfortunately, being structurally disordered, the high quality, unambiguous characterization of their short, middle and extended-range structural scales is an extremely difficult task.

Thanks to the significant technical and methodological progresses made during the last decade, solid state NMR has now become the only method that can accurately define the atomic structures of disordered, heterogeneous and amorphous materials. However, the interpretation of the rich indirect information, that can be inferred from the analysis of the experimental spectra, is only rarely straightforward because of the overlapping sub-spectra of the different structural units present in the glass.[3–8]

The calculation of the NMR parameters from first principles has recently become possible for large infinite solids described within periodic boundary conditions, plane wave basis sets and density functional theory. In this framework, Pickard and Mauri in 2001 developed the gauge including projector augmented wave (GIPAW) method,[9] which proved very quickly to exhibit an outstanding accuracy and to overcome the limitations of the cluster approximation used in earlier theoretical investigations.[10–16] Moreover, recent advances have allowed us to go beyond the determination of the spectroscopic parameters, computationally simulating the line widths and shapes of the NMR spectra. This makes a direct comparison with experimental observables at least possible and remarkably facilitates the interpretative process.[17,18] A couple of comprehensive reviews on first principles calculations of NMR parameters by means of the GIPAW approach have appeared very recently.[19,20] Both are largely focused on the theory behind the calculation of all-electron NMR parameters in solids and on current methodological advances in solid state NMR. Applications to a large variety of chemical systems are thoroughly discussed whereas oxide glasses are only briefly described.

The present review aims to (a) increase the awareness of the recent advances in the integrated computational strategies available, to compute solid state NMR parameters and simulate one and two dimensional NMR spectra; (b) prove the decisive role of crossovers among experiments, computations and theoretical models, for a deeper understanding of the spectral behavior associated with complex systems, such as disordered multicomponent inorganic materials; (c) facilitate the effective application of these techniques to common problems encountered in oxide glasses and (d) provide a practical guide to scientists who wish to empower their research with computed chemical shifts and simulated spectra.

For these reasons it is hoped that the review will be of direct relevance to both computationally and experimentally oriented researchers working in the field of chemistry, physics, and material chemistry as well as graduate students and newcomers to this hot topic.

After a brief overview of the basic features of oxide glasses and of the experimental techniques routinely employed to investigate their structure, a general description of the computational methods usually adopted to generate sound structural models of amorphous materials is offered. This section is followed by the presentation of the computational recipe used to compute the solid state NMR spectra of oxide glasses and to establish quantitative structural-NMR property relationships which are fundamental to gain new insight into the structural role of the different components of glasses directly from NMR experiments, through a structural inversion method. Finally, these concepts are applied to 'simple' network former glasses such as vitreous SiO_2, B_2O_3, GeO_2 and Al_2O_3 and more complex silicates, aluminosilicate, phosphosilicate and borosilicate glasses of scientific relevance.

The final section is dedicated to the future developments that will hopefully help the computational approach described to overcome some of the current limitations.

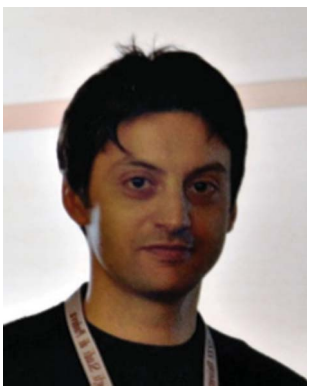

Alfonso Pedone

Alfonso Pedone received his degree and Ph.D. in Chemistry at the University of Modena and Reggio Emilia where he became a researcher after a 2-year post-doctoral position at the Scuola Normale Superiore of Pisa. He conducts research in the field of computer simulations based on classical and quantum methods applied to the study of inorganic materials and nanomaterials for applications in the field of nano-medicine, energy conversion and confinement of radioactive waste. He has co-authored about 49 papers published in international journals and 3 book chapters. He has received more than 600 citations and has an h-index = 16.

2. Glass structure determination: the limits and beyond

2.1 The structure of oxide glasses

The structure of oxide glasses is an archetypal example of a continuous random network of coordination polyhedra made of network-forming cations (such as Si, P, B, Ge, *etc.*) and oxygen (see Fig. 1(a)).[21–23] Bond lengths and angles of the polyhedra vary only over a narrow range and, together with the cation coordination number, describe the so-called short range structure of the glass. Cation–oxygen polyhedra, like SiO_4 in vitreous silica or BO_3 in vitreous boron oxide, are usually corner-linked through 'bridging' oxygens (BOs). Structural disorder in a glass network arises from the statistical distribution of angles and unconstrained dihedral angles between the coordination polyhedra compared to those in crystals.[23]

Addition of network-modifying alkali and/or alkaline-earth ions has been shown to break-up the connectivity of the oxide network with the creation of terminal anions, called non-

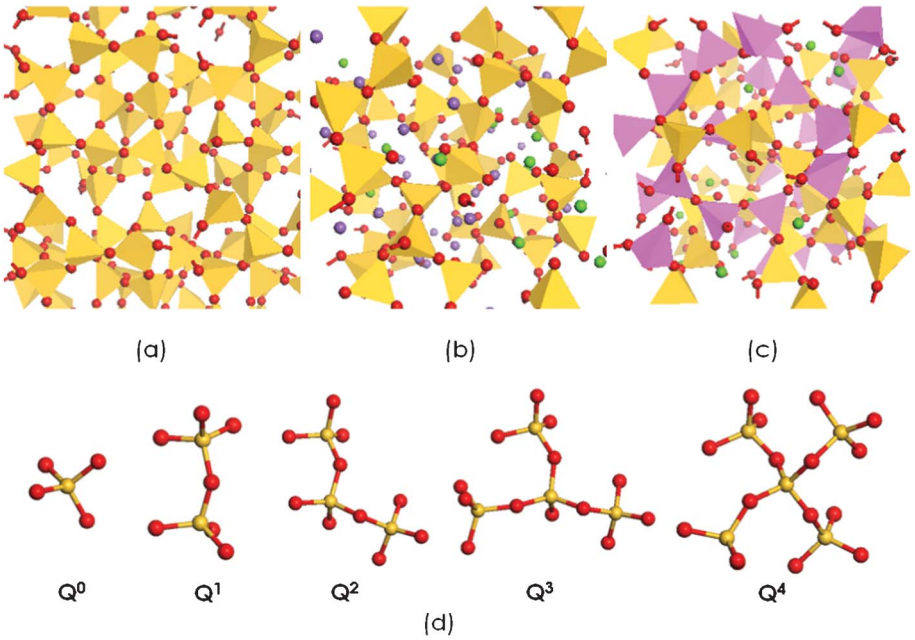

Fig. 1 Three dimensional representations of the random network structural models of oxide glasses. (a) Continuous random network model of silica glass; yellow tetrahedra represent SiO_4 units and red spheres represent oxygen atoms. (b) Modified random network model of a soda–lime silica glass; green and violet spheres represent calcium and sodium ions, respectively. (c) Compensated continuous random network model of an aluminosilicate glass; magenta tetrahedrals represent AlO_4 units. Finally, (d) three dimensional representations of the different Q^n species (central atom).

bridging oxygens (NBOs), that are linked to only one network-forming cation.

The medium-range configuration around the network-forming cation is expressed as Q^n (n = 0–4), where Q designates 'quaternary' and n the number of BO oxygens connected to other network former cations. (Fig. 1(d)) The quantification of the Q^n species therefore provides a direct link to the polymerization degree of the structure. Thus, Q^4 describes a three-dimensional network, Q^3 two-dimensional sheets, Q^2 chains and rings, and Q^1 and Q^0 correspond to isolated dimers and tetrahedra, respectively. The resulting structure can be envisaged as a combination of a partly depolymerized network and ionically packed modifying oxides. According to the modified random network model[24] at high concentrations, the modifiers percolate through the bulk of the glass and form primary pathways, or channels, which play a key role in important properties of glasses. (Fig. 1(b))

When tetrahedral network formers, like Al, are introduced into a modified silicate glass composition they predominantly form negatively charged $(AlO_{4/2})^{1-}$ units that are charge compensated by the modifying cations and the concentration of non-bridging oxygens is reduced in proportion. Geometrically, a compensated continuous random network[25] should return into an aluminosilicate glass with a tectosilicate composition, that is for an equimolar ratio of alkali or alkaline-earth oxide and Al_2O_3, as illustrated in Fig. 1(c).

This ''cation centric'' view needs to be complemented by a description of the local environment of the oxygen which is the volumetrically and numerically the predominant ion in oxide glasses. From the oxygen side, the structure of silicate glasses can be described by the distributions of the framework (network former) and non-framework (network modifiers or charge balance) cations around itself.[26] Various degrees of topological and/or chemical disorder can be highlighted.[27] Topological (or geometrical) disorder refers to the distribution of bond lengths and bond angles. Chemical disorder is based on the distribution of mixing compositional units and refers to: (i) the connectivity, which quantifies the extent of mixing among framework units alone, (ii) the degree of polymerization, which refers to the intermixing of framework and non-framework cations controlling the distribution of NBOs, and (iii) the non-framework disorder, which denotes the distribution of network modifying or charge balancing cations.

2.2 Advanced techniques for glass structure determination

In the last decade significant advancements have been achieved in the understanding of the atomic structure of oxide glasses thanks to the improvements in several experimental methods, like extended X-ray absorption fine structure (EXAFS) spectroscopies, elastic and inelastic neutron and X-ray scattering, small-angle and wide-angle X-ray scattering (SAXS/WAXS), infrared and Raman spectroscopy, and solid state nuclear magnetic resonance (NMR).[23]

2.2.1 Diffraction techniques. Diffraction data can be used to determine atomic structures by creating and refining structural models. Well-defined diffraction spots that represent reflections off the repeating lattice of atoms are found for single crystals. On the contrary, for amorphous materials the amount of information decreases rapidly with distance, and answers to structural questions must be cast in probabilistic rather than deterministic terms. The data collected are transformed into a radial distribution function (RDF) that

provides the distribution of interatomic distances, typically over the range of 1 to 10 Å. Depending only on two-atom (''pair'') correlations, the bond and torsion angle distributions cannot be obtained directly from the RDF without at least a few starting assumptions. Hence, the resulting distributions are only as good as the chosen assumptions.

Although the lack of uniqueness of the RDF beyond very short range structures (beyond 5 Å) has been recognized, the RDF has still been repeatedly used to make structural inferences because it had been generally assumed that no competing non-random network model could fit the data equally well.[28,29]

2.2.2 Solid state NMR. Substantial progresses in solid state NMR methodologies, particularly during the 1990s, have rendered this technique an immensely powerful tool for the conceptual description of structural and dynamic disorder in glasses. Since only the local environment of the particular nucleus under study is probed by NMR, this method is especially well-suited for the structural analysis of highly disordered and compositionally very complex systems, where diffraction techniques, IR and Raman spectroscopy often fail or do not provide sufficient results.[3–5]

The directional character of many NMR interactions coupled with the rigidity of structural units in non-crystalline solids results in heavily broad line-shapes, which can be envisioned as being composed of a series of narrow lines, each coming from a different crystallite orientation with respect to the external magnetic field. For this reason, more effort over the last 40 years has been devoted to the development of ways to average out this anisotropic broadening, either by manipulating the spins with radiofrequency pulses or by sample motions. Initial experiments were focused on magic angle (sample) spinning, MAS, which has been extensively applied to cancel out the effect of the dipolar and chemical shift anisotropies of spin 1/2 nuclei (such as ^{29}Si) in silica-based glasses.[30–33] However, MAS fails to remove the second-order quadrupolar effects present for nuclei with a half-integer nuclear spin (so-called half-integer quadrupolar nuclei, ^{17}O (I = 5/2), ^{43}Ca (I = 7/2), ^{27}Al (I = 5/2), ^{11}B(I = 3/2) and ^{23}Na (I = 3/2)) and quadrupolar coupling constant of the order (or larger than) ~MHz; therefore, new techniques such as dynamic angle spinning (DAS), double rotation (DOR), or multiquantum magic angle spinning (MQMAS) have been developed.[34–37] The latter has now become a standard technique in the NMR toolbox whereas the two formers are much less commonly applied as being much more technically demanding.

Important strengths of modern high-resolution NMR can be summarized as follows: (a) NMR is element-specific, *i.e.* it allows the exclusive investigation of the local environment of the atom of interest (providing that it bears a nuclear spin), distinguishing between various constituent structural units and determining the nature of the nearest and next-nearest neighboring atoms and atomic coordination; (b) this technique shows high sensitivity to small variations in the first and second coordination sphere of the observed nucleus; (c) as opposed to other spectroscopies, NMR may characterize glass structures not only over an atomic scale ($\leqslant$0.3 nm) but can also assess their intermediate-range order up to nearly 1 nm[4,38–41] (NMR provides now a wealth of techniques to probe spatial proximities[42] or chemical bonds between atoms[38]); (d) the direct proportionality of the signal intensity to the number of contributing nuclei makes NMR the method of choice for stringently quantitative applications whenever bulk information is required; (e) moreover, compared to several other methods, NMR is non-destructive and requires little sample preparation (typically 100 mg). Finally, by choosing appropriate experimental protocols, highly specific information can be obtained. A combination of several such experiments can then yield a wealth of complementary information about various aspects of the structural problem under study.[38–40]

2.2.3 Computational approaches: beyond the cluster approximation. The detailed structural information provided by NMR (such as the connectivity, distances or bond angles with neighboring atoms) cannot be extracted from the spectra without a good understanding of the structural significance of NMR parameters. This can be achieved either empirically by reference to materials of a known structure or theoretically using *ab initio* calculations. The first approach has been extensively applied in silicates for ^{29}Si NMR,[43] ^{17}O NMR,[13,44,45] and ^{23}Na NMR,[12,46–49] for ^{27}Al NMR,[50,51] ^{11}B NMR[52,53] and other nuclei.[36] However, crystalline systems generally exhibit a limited diversity of local structures in contrast to the disorder and variety of structural units (different coordination numbers and Q^n distributions) present in multicomponent glasses. *Ab initio* calculations in silicates using model clusters were pioneered by Tossell and co-workers[15,16,54,55] for ^{29}Si and ^{17}O NMR. These calculations have exhibited trends in the geometrical parameters of the tetrahedral linkage that correlate well with experimental data[10,11,14,56–60] and have been particularly useful in quantifying structural distributions in silicate glasses from NMR data.[61–64]

The rational for the cluster approach lies in the fact that NMR parameters are essentially local properties and are therefore dominated by bonding in the first few coordination spheres. The accuracy of this approach is limited mainly by the choice of the correct basis sets for the atomic orbitals, the size of the cluster, the termination of the dangling bonds produced on cutting the cluster from the infinite solid (for covalent solids) and the treatment of the electrostatic interactions.[65–68] Moreover, in the special case of amorphous materials, the cluster approach does not account for the correlations between structural factors that exist in solids and disorder in glasses. Furthermore, calculations of the NMR properties of non-bridging oxygens (NBOs) are much more demanding than those of bridging oxygens (BOs), as they require model clusters of a much greater size to achieve sufficient accuracy. Indeed, the cubic scaling with the number of atoms severely limits this kind of calculations. These limitations are certainly the reason why so few attempts have so far been made on multicomponent glasses.[10,60,69,70]

To overcome these limitations several efforts to obtain a quantitative comparison between information derived from NMR spectra and structural features obtained from molecular dynamics (MD) simulations have been published. They mainly focused on the connectivities between different types of Q^n species and related descriptors,[31,64,71–80] but attempts to investigate cation distribution and clustering have also been made.[33] Moreover, the interpretative and predictive relevance

of statistical correlations between NMR-derived and MD-derived descriptors (quantitative structure–properties relationships) has been discussed.[81,82]

The introduction of effective methods specially devised to calculate NMR parameters in large systems described within periodic boundary conditions, plane wave basis sets and density functional theory have solved most of the aforementioned problems. In this framework, chemical shifts and electric field gradients are obtained from first principles with the gauge including projector augmented wave (GIPAW) and the projector augmented wave (PAW) methods, respectively.[9,83,84] The outstanding accuracy of these DFT methods has been demonstrated recently for various crystalline and amorphous solids.[83,85–97]

However, often in the case of oxide glasses and melts, the theoretical determination of NMR parameters is not sufficient for a direct comparison with experimental observables, since the latter ones are usually derived from the empirical fitting of the NMR spectra,[63,98,99] which are composed of several overlapping broad peaks of the different structural units present in the glass.[3,100] A possible solution for a direct comparison between theory and experiments, and thus for a detailed interpretation of solid state spectra aided by computer experiments, is to employ the computed NMR parameters to model the whole spectra by means of a spin-effective Hamiltonian encoded in homemade packages, as recently developed by Charpentier.[17,18]

2.2.3.1 Glass structure generation by classical and ab initio molecular dynamics—a brief overview. Classical Molecular Dynamics. Classical MD is well established as a powerful tool to provide an atomic scale picture of the structure of glasses and an improved understanding of composition-atomic structure relationships. In this approach, the glass structure is represented by a classical ensemble of particles described using empirical force fields.[101] The initial configurations are generated with a random distribution of atoms in cubic simulation boxes, with the atom numbers and box dimensions consistent with the experimental composition and glass density. To compensate for a faulty assumption of periodicity, large unit boxes comprising thousands of atoms are needed. Bulk glasses are usually made *via* a simulated melt–quench technique. The system is initially held at a constant volume at high temperature for tens to hundreds of picoseconds in order to simulate a liquid structure. The melt is then cooled through the glass transition temperature down to room temperature, and equilibrated. The statistical ensemble (NVE, NVT or NPT) used in the procedure is an element of choice. Cooling of the melt can occur *via* several protocols based on lowering the temperature continuously or by large steps in which the system undergoes an instantaneous decrement followed by a relaxation period. A nominal cooling rate typically of 5–10 K ps^{-1} is usually adopted.[102,103] Theses procedures are depicted in Fig. 2.

The time evolution of each particle in the ensemble is followed by solving Newton's equations of motion with an iterative process: positions and velocities are updated in small increments of time, known as time steps. Each increment corresponds to a time step of the order of 10^{-15} s. The

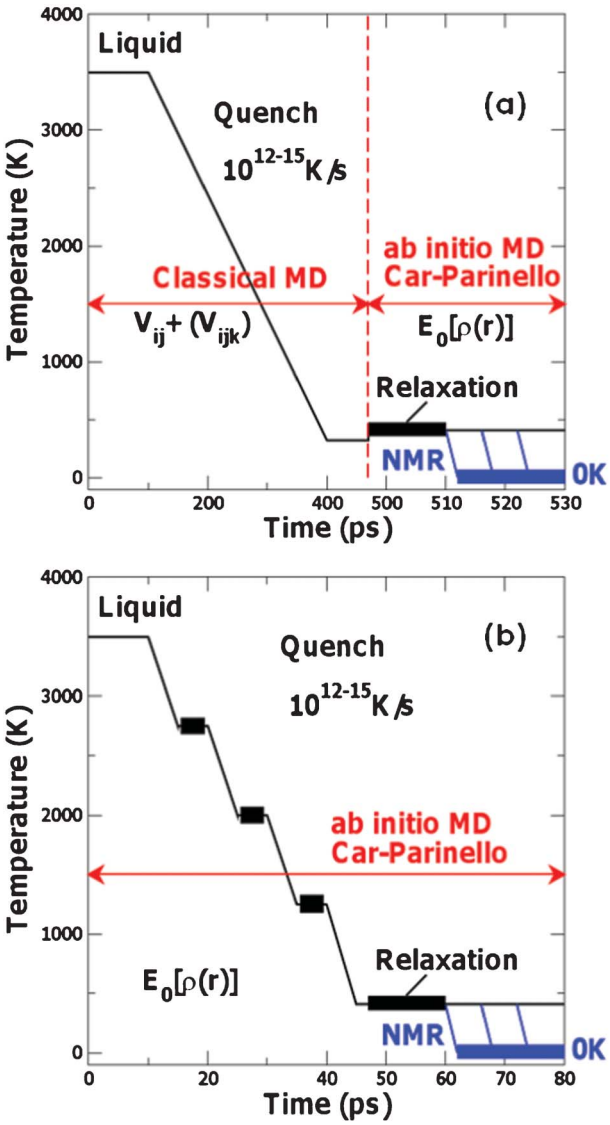

Fig. 2 Schemes of the cooling protocol adopted for generating structural models of glasses *via* mixed classical–*ab initio* molecular dynamics (a) or full *ab initio* molecular dynamics (b).

structure of the glass is obtained by averaging over a large number of time steps, of the order of thousands or hundred-thousands.

Usually, the Born model of the solid is used for calculating the forces that act on the atoms. Atoms are treated as point charges with short-range potentials acting on them[104] and more accurate results can be obtained by including many body effects.[105] The shell-model potential is a more accurate and efficient way to take the molecular environment into account.[106] Here, the atomic polarizability is explicitly incorporated in the model by replacing polarizable atoms (typically the oxide ions for silicates) with core–shell dipoles consisting of two opposite charges connected by a harmonic spring.[107–110] The short-range potentials are given in terms of parameterized analytical functions and include both repulsive (due to Pauli repulsion) and attractive (due to dispersion) terms. The magnitudes of the

point charges are also model parameters; the formal oxidation state charge is used for ionic solids, whereas for materials in which the bonding has a more covalent character reduced partial charges may be used. Interatomic potential models are usually parameterized to reproduce experimental or accurate *ab initio* data on cluster or periodic systems.[104,111–113] Despite an overwhelming success (which will however not be praised in this review), the need to devise interatomic potential models implies serious drawbacks especially when the interest is shifted from simple silicate based compositions towards the modeling of multicomponent compositions of oxide glasses. In fact, often the transferability to systems or regions of the phase diagram different from the ones to which they have been fitted is restricted. While the obtained short-range structure seems to be predominantly governed by the interatomic potential parameters,[114,115] the cooling procedure was found to affect the medium range structure, specifically in the population of the different ring size distributions and in the number of defects formed.[103,116,117]

In summary, the accuracy of the results of the simulations is affected by: (a) the interatomic potential parameters, (b) the cooling rate used to obtain the glass which is several orders of magnitude faster than the physical one, (c) the limited size of the system (typically consisting of thousands of atoms) which, in turn, limits the structural relaxation, and (d) the fictitious structural constraints enforced by the periodic boundary routinely employed to remove surface effect. All these factors might lead to a final model with a higher artificial temperature than the corresponding experimental composition.[103,118,119]

Ab initio molecular dynamics. It is generally assumed that the main limitations of classical MD may, in principle, be overcome by the *ab initio* molecular dynamics (AI MD) method. Indeed, this method does not require the derivation of empirical parameters, as the forces acting on the nuclei computed from electronic structure calculations that are performed ''on the fly'' as the molecular dynamics trajectory is generated. In this way, the electronic variables are not integrated beforehand, but are considered as active degrees of freedom. This implies that, given a suitable approximate solution of the many-electron problem, also relatively large systems can be handled by molecular dynamics. But this also implies that the approximation is shifted from the level of selecting the model potential to the level of selecting a particular approximation for solving the Schrödinger equation.

Set in the framework of density functional theory (DFT),[120] the Car–Parrinello (CP) approach to AI MD[121] provides an algorithm that is very efficient from the computational point of view. In fact, the updating of the electronic degrees of freedom for each ionic configuration visited during the MD trajectory does not involve explicit minimization of the electronic density functional, as in Born–Oppenheimer MD.[122] The basic idea is to introduce fictitious Newtonian dynamics for electrons that are then considered as additional, fictitious degrees of freedom whose motion is dynamically coupled to the real ionic motion.[123]

The glass structure obtained by AI MD melt-and-quench furnishes an unbiased view of some structural and dynamical features of glasses, such as the role of coordination defects in the glass-forming process and the mechanism of interchange between Q^n species, as well as the assessment of the actual occurrence of specific structural features such as intermixing cations in network polymerization or the presence of tricluster oxygens in the glass. However, the increased accuracy and predictive power of AI MD simulations comes at a significant computational cost. The system size (100–300 atoms), correlation lengths and relaxation times (10–100 ps) that are accessible are much smaller than what is affordable *via* classical MD. Therefore, these methods would hardly produce a statistically sound description of medium-range features in silicate glasses containing more than four oxides.

Mixed classical–AI MD procedure. A common approach in first principles simulations of glasses is to obtain an initial structure through classical MD with an empirical potential and then switch to the *ab initio* treatment using the classical structure as a 'starting guess'.[124–127] This allows a partial relaxation of the structure at the *ab initio* level, but some important structural features, such as the inter-tetrahedral connectivity and the composition of the ionic coordination shells (medium-range structure), will hardly be changed upon switching to the *ab initio* treatment, and therefore they remain completely determined by the quality of the empirical potential used to construct the initial structure. This limits the scope of these mixed classical–*ab initio* approaches to investigate short-range features, or properties which turn out to have a mainly local character such as IR–RAMAN and NMR spectra.[93,94,124–126,128–131]

3. NMR parameter calculation and spectra simulations

3.1 The MD–GIPAW method, a brief overview

The chemical shift and the electric field gradient interactions for each atom in the (super)cell are obtained from first principles with the gauge including projector augmented wave (GIPAW)[9] and the projector augmented wave (PAW) methods,[83,132] respectively. They are obtained as matrices (which is the direct consequence of their directional character) and the transformation to experimental parameters (relative orientation with the crystallographic axes, isotropic part, anisotropy and asymmetry parameter) has been thoroughly described in ref. 17.

Briefly, the isotropic chemical shift, δ_{iso}, is obtained from the isotropic magnetic shielding, σ_{iso}:

$$\sigma_{iso} = {}^1\!/_3 Tr\left\{\overleftrightarrow{\sigma}\right\}$$

through:

$$\delta_{iso} = -(\sigma_{iso} - \sigma_{ref})$$

where σ_{ref} is a reference isotropic shielding (generally computed using a set of crystalline reference compounds). The anisotropy of the symmetrized tensor $\overleftrightarrow{\sigma}$ is characterized by the chemical shift anisotropy (CSA), δ_{CSA}, reflecting its magnitude and by an asymmetry parameter, η_{CSA} describing its deviation from cylindrical symmetry ($\eta_{CSA} = 0$):

$$\delta_{CSA} = \delta_{ZZ} - \delta_{iso}$$

$$\eta_{CSA} = \frac{\delta_{YY} - \delta_{XX}}{\delta_{CSA}}$$

Where δ_{ii} are the principal components (*i.e.* the eigenvalues) of the symmetric chemical shift tensor, such that $|\delta_{ZZ} - \delta_{iso}| \geq |\delta_{XX} - \delta_{iso}| \geq |\delta_{YY} - \delta_{iso}|$.

Similarly, the quadrupolar interaction is characterized by a coupling constant C_Q and an asymmetry parameter η_Q, which are related to the electric field gradient tensor through:

$$C_Q = \frac{eQV_{ZZ}}{h}, \text{ and } \eta_Q = \frac{V_{XX} - V_{YY}}{V_{ZZ}}$$

where V_{xx}, V_{yy} and V_{zz} are the principal components of the electric field tensor defined, such that $|V_{ZZ}| \geq |V_{YY}| \geq |V_{XX}|$, and Q is the nuclear electric quadrupole moment. Its value is either taken from literature[133] or using reference compounds (fitting the computed V_{zz} to the experimental C_Q values). The theory and methods supporting the calculation of all-electron NMR parameters in solids with the PAW and GIPAW approaches have been very recently exhaustively reviewed, therefore it is not discussed in the present review.[19,20]

The GIPAW method combined with molecular dynamics simulations (hereafter referred to as the MD–GIPAW approach) provides the missing link between the variations of the local structure of disordered solids and the experimental distributions of the NMR parameters.[85,86] In fact, with sufficient statistics provided by MD models one can seek for the relationships between NMR parameters and local geometries, the range of the latter not being constrained by the crystalline state. Thus, the MD–GIPAW approach has opened new routes for interpreting NMR parameter distributions, refining relationships between NMR parameters and local structural features. The accuracy of the structural models obtained is in turn demonstrated by the consistency of the theoretical and experimental NMR parameters and spectra. Most importantly MD–GIPAW, with the help of statistical tools, enables the direct comparison between NMR experimental and MD data (through the theoretical NMR spectrum), thus allowing further assessment of structural models and of the theoretical parameters (force fields) underlying the MD simulation.[19]

For the sake of clarity in the remainder of the text, theoretical and simulated spectra refer to the calculated spectra using NMR parameters from the MD–GIPAW calculations and from the fit of the experimental data, respectively. Theoretical NMR parameters refer to the parameters obtained from MD–GIPAW NMR calculations, whereas predicted NMR parameters are those obtained from the quantitative structure–NMR parameter relationships.

The computational protocol typically employed is shown in Fig. 3; it consists of several steps: (a) classical MD simulations are employed to generate the structural models of the glasses of interest; (b) periodic DFT first principles calculations coupled with GIPAW algorithm are employed for geometry relaxation and the calculations of the NMR parameters (chemical shielding and quadrupolar parameters) of each atom of the model; (c) spin-effective Hamiltonians encoded into a dedicated software named fpNMR[17,18] are employed to simulate the solid state 1D and 2D NMR spectra directly comparable with the experimental counterparts; (d) comparison between experimental and theoretical parameters is performed; (e) if the results of the comparison in point (d) is satisfactory it is possible to proceed to the comparison between the simulated and theoretical spectra, and to the establishment of quantitative structure–NMR parameter relationships. Otherwise, either the information obtained can be used to improve the 3D model or, equally important, to plan and perform appropriate experiments in order to exploit each technique to its fullest potential.

Once obtained, sound quantitative structure–NMR parameter relationships can be used to reconstruct the structural parameter distribution from the NMR spectra through the so called ''structural inversion'' method.[18]

3.2 The MD–GIPAW method—main limitations

It is worth highlighting that the success of the results obtained by this protocol and the discrepancies often encountered in points (d) and (e) are intimately related to the limitations of the first three steps. As already stated, the first cause of a disagreement between theory and experiments could be imputable to the accuracy of the structural model on which the NMR calculations are performed. To obtain final unequivocal proof of ''computational defects'' possibly generated in the three dimensional model of the glass, *i.e.* structural features not present in the real structure, the exact knowledge of where the signal of these units lies in the spectrum is needed.[92–94,125]

Among the limits of the structural models employed up to now, it is worth mentioning the effect of the system size that limits the statistics of the structural and NMR results. Because of the dominant local character of the NMR interactions, system sizes starting from 100 atoms have been found to be sufficient to predict NMR parameters.[17,92] To overcome the limitations in the number of atoms for the simulation of NMR spectra, the kernel density estimation (KDE) approach has been proposed and found to be particularly efficient for MQMAS spectra.[17,18,134] However, the continuous increase of computing power and algorithmic efficiency will shortly make larger and more realistic systems amenable to first principles NMR calculations, allowing the investigation of fine structural changes resulting from long range interactions (such as packing effects). In addition, efficiency gain in the AI MD methodology will also address more satisfactorily the limitation of the numerical quench rate.

Other discrepancies are inherently related to the limitations of the density functional theory and its implementation for the computation of NMR parameters. For example, at present the GIPAW calculations are limited to functionals of the GGA (generalized gradient approximation) type like PBE[135] and PW91.[136] Furthermore, the use of reliable pseudopotentials, whose transferability and accuracy must be checked against both the prediction of structural and NMR properties. is of crucial importance.[137] Reliable norm-conserving and ultrasoft pseudopotentials are usually available in libraries provided with DFT software packages like CASTEP[138] and Quantum

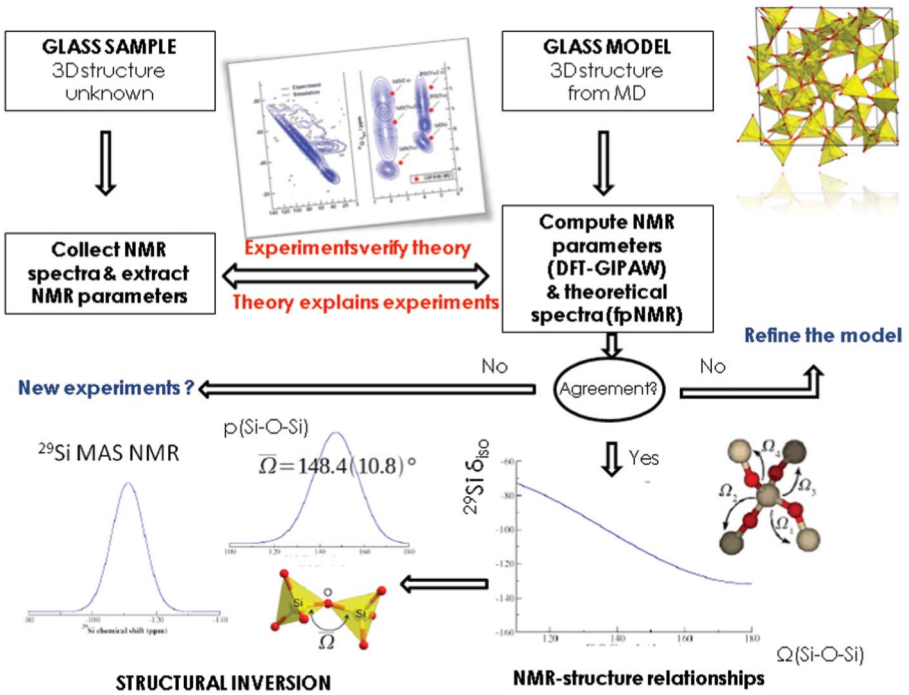

Fig. 3 Schematic description of the steps employed in the MD–GIPAW computational procedure to elucidate the structural features of oxide glasses.

Espresso.[139] However, sometimes the standard pseudo-potentials are not accurate enough or the DFT approach fails to reproduce the correct energy of atomic orbitals in all electron calculations, thus the energies of the pseudo wave functions are badly fitted during pseudopotential generation. For example, it has been demonstrated that when using PBE exchange correlation functionals for the treatment of the cationic localized empty orbitals of Ca^{2+}, Sc^{3+} (3d) and La^{3+} (4f), a correction is needed to calculate accurately the ^{19}F and ^{17}O chemical shieldings.[86,140] This correction consists in a shift of the energy levels of the unoccupied orbitals to match the experimental chemical shifts of the ions in different environments.

GIPAW calculations provide the shielding and electric field gradient tensors of all atoms in the system. As described above, two parameters must be supplied by the user, a reference isotropic shielding σ_{ref} and a nuclear quadrupole moment Q to obtain the related values, that is the isotropic chemical shift δ_{iso} and the quadrupolar coupling constant C_Q. Both σ_{ref} and Q are generally treated as adjustable parameters that depend on the functional and the pseudopotentials employed in the calculations.

Moreover, an additional source of discrepancy between the calculated and experimental NMR parameters may be found in the fact that the latter are collected at room temperature while the former are usually computed on a single static structure (generally representative of a 0 K temperature). Therefore, the inclusion of thermal and motional effects could be needed in certain cases.[141–143] Two methods are up to now envisaged to include this correction. The first one consist in a vibrational averaging of the property with respect to normal modes populated according to a Boltzmann distribution at the temperature of interest.[141,143] In this case, the normal modes and frequencies of vibrations are calculated within the harmonic approximation and the unharmonic effects could be included by using second order perturbation theory. The second approach, in which unharmonic effects are intrinsically accounted for, relies on the generation of a set of configurations by extracting snapshots from MD simulations at the temperature of interest.[142,143] The 'temperature-corrected' NMR parameter is then obtained by averaging over snapshots whose total number and time spacing between them must be large enough to reach fully converged and uncorrelated values. This has been addressed partially using Langevin MD to accelerate the phase–space sampling.[144] However, these correlation effects open appealing perspectives such as the prediction of NMR relaxation properties from first principles.[144]

4. Network forming oxides

4.1 Vitreous silica

Vitreous silica has been intensively investigated by using both ^{29}Si and ^{17}O NMR since the mid 1980s with the aim of finding relationships between NMR parameters and structural features such as Si–O distance and Si–O–Si bond angle distributions.[57,58,145,146] Experiments on crystalline phases and theoretical investigations on cluster models of silica have revealed that the isotropic ^{29}Si δ_{iso} tends to increase (*i.e.* become less negative) as the Si–O internuclear distance increases, and/or as the Si–O–Si bond angle decreases.[147] As for the ^{17}O NMR parameters, the ^{17}O δ_{iso} and η_Q both increase

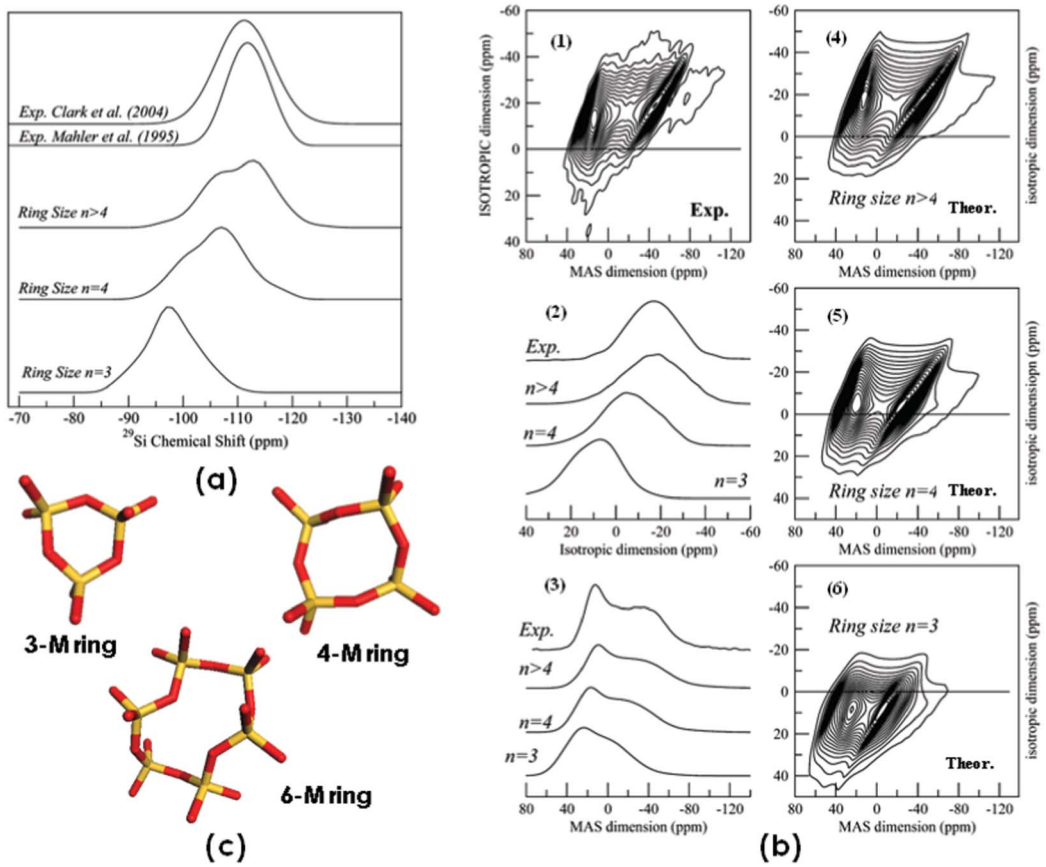

Fig. 4 (a) Comparison between experimental ^{29}Si MAS NMR spectra of vitreous silica and the theoretical ^{29}Si MAS NMR spectra of three-, four- and other *n*-membered rings. (b) Experimental (1) and theoretical ^{17}O DAS NMR spectra of (6) three-, (5) four- and (4) other *n*-membered rings. Panels (2) and (3) report the comparison between experimental and theoretical isotropic and MAS dimension projections, respectively. (c) Three-, four- and six-membered rings in vitreous silica. Figures (a) and (b) are reprinted with permission from ref. 18 (refer for details), copyright 2009 American Chemical Society.

with the decrease of the Si–O–Si angle, whereas C_Q shows an opposite trend.[58,145,146] Moreover, whereas δ_{iso} and C_Q depend both on the Si–O distance and Si–O–Si bond angle, η_Q is related only to the bond angle.[58,145,146]

The first application of the GIPAW approach to vitreous silica was reported by Charpentier *et al.*,[18] who simulated and interpreted the ^{17}O DAS and ^{29}Si MAS NMR spectra of structural models of vitreous silica generated by a hybrid MC–MD simulation, and discussed the implication of the ring size distribution on glass density. They showed that the NMR parameters (C_Q, η_Q and δ_{iso}) of ^{17}O and δ_{iso} of ^{29}Si in *n*-fold ring species with $n > 4$ are in better agreement with experiments with respect to the ones generate with smaller rings, thus indicating a very low concentration of small rings in vitreous silica. Fig. 4 highlights and summarizes some of the results obtained in this pioneering work.

Strong correlations between the ^{17}O quadrupolar NMR parameters were observed. These correlations were shown to govern the line shape of the ^{17}O DAS NMR spectrum[146] and had therefore to be taken into account for fitting with high accuracy the experimental data. Moreover, a strong dependence of each of the ^{17}O NMR parameters (C_Q, η_Q and δ_{iso}) upon the Si–O–Si angle has also been highlighted (Fig. 5(a)) and a new structural inversion model has been presented and applied for the reconstruction of the Si–O–Si angle distribution from the ^{17}O DAS NMR spectrum (Fig. 5(b)).

Finally, the reliability of the whole procedure was demonstrated conclusively by the results of the structural inversion method to reconstruct the Si–O–Si bond angle distribution independently from the ^{17}O and ^{29}Si NMR spectra by obtaining Si–O–Si angle distribution mean values of 147.1° and 148.4°, respectively, and standard deviations of 11.2° and 10.8°, respectively.

4.2 Vitreous B_2O_3

The structure of vitreous B_2O_3 has been long the subject of a controversy regarding the concentration of hexagonal $B_3O_{9/2}$ units, named boroxol rings.[148] Early NMR experiments highlighted the presence in both ^{11}B NMR and ^{17}O NMR spectra,[8,149–152] of two populations which were assigned to atoms inside and outside the rings by calculations of cluster models[153,154] and by comparison with borate crystals of known structure.[52] The fraction of boroxol rings (*f*) determined in these studies ranges from 65% to 85%. No consensus has been observed among the results of reverse Monte Carlo,[155] classical,[156,157] and first principles[158,159] simulations which have furnished values of *f* ranging from <30% to 75%.

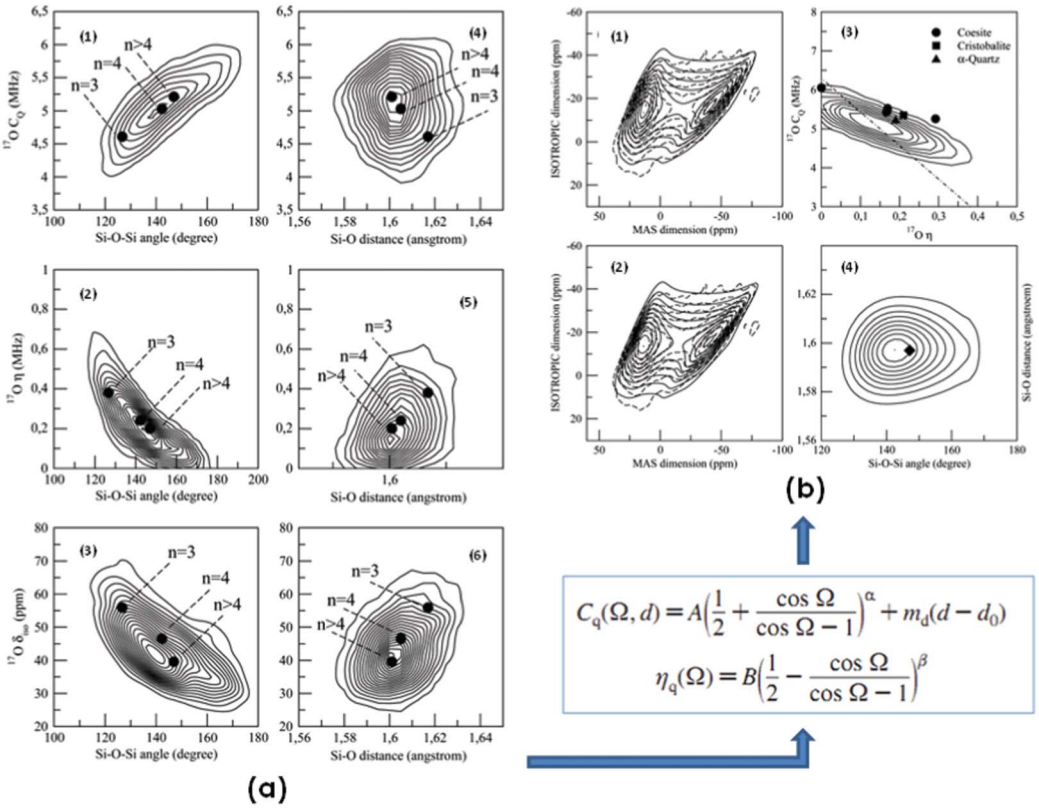

Fig. 5 Contour plots of theoretical two-dimensional distributions (1) p(C_Q,Ω), (2) p(η_Q, Ω), (3) p(δ_{iso}, Ω), (4) p(C_Q,d), (5) p(η_Q,d) and (6) p(δ_{iso},d) for the oxygen atoms in the model structures of vitreous silica. Ω is the Si–O–Si bond angle, and d is the Si–O bond distance. Solid circles represent the averaged values over all model structures for three-, four-, and other n-membered rings. (b) Comparison between the fit (solid lines) and experimental (dashed lines)[146] ^{17}O DAS NMR spectra using (1) Clark's method[146] and (2) Charpentier's method[18] (see references for details). (3) Comparison between the distribution p(C_Q,η_Q) obtained from the fit (1) (dotted–dashed lines) and fit (2) (solid lines). Experimental values of (C_Q, η_Q) for crystalline silica polymorphs are also shown. (4) The theoretical distribution of the Si–O–Si bond angle and the Si–O bond length obtained from the distribution of (C_Q,η_Q) displayed in (3) (solid lines). The mean value of (Si–O–Si, Si–O) is also shown (4). Figures (a) and (b) are reprinted with permission from ref. 18 (refer for details), copyright 2009 American Chemical Society.

In 2008 Ferlat *et al.*[88] applied the MD–GIPAW approach to compare the ^{11}B DAS (isotropic projection) and ^{17}O MAS NMR spectra calculated by first principles MD for three dimensional models of boroxol-poor (BP) and boroxol-rich (BR) glasses with the corresponding experimental spectra. The results allowed a straightforward discrimination between the two boron species, in fact although the two models lead to similar neutron diffraction data, only boroxol-rich models, (with a fraction of boron atoms of 75%) reproduced the full set of NMR observables.[88]

4.3 Vitreous GeO_2

Whereas the short-range order in vitreous GeO_2 has been well characterized by diffraction experiments and is determined by the GeO_4 tetrahedra units as in crystalline quartz GeO_2, the medium-range structure which is usually described by the distribution of Ge–O–Ge bond angles is still a subject of debate. Neutron diffraction experiments have suggested an average Ge–O–Ge bond angle of 132° but since the investigation of medium-range order is notoriously difficult for diffraction probes, recent studies have been based on NMR spectroscopy for which, however, NMR structure–property relationships are needed.

The correlations between experimental NMR parameters and the underlying structural properties, in particular the Ge–O–Ge bond angles, have been investigated by Kibalchenko *et al.*[160] by making use of atomistic model structures of vitreous GeO_2 generated by classical and first principles simulation methods. The full set of ^{73}Ge NMR and ^{17}O NMR parameters (δ_{iso}, C_Q and η_Q) have been determined by means of the GIPAW approach. Clear correlations have been established between ^{73}Ge NMR δ_{iso} and the mean of the neighboring Ge–O–Ge bond angles, and between ^{17}O NMR C_Q, and η parameters and the local Ge–O–Ge angle. By combining the available experimental data for C_Q in vitreous GeO_2[161] and the corresponding correlation obtained, the authors have identified the range of variation of the Ge–O–Ge bond angle in the glass (124°–139°) and the mean bond angle (135°) in agreement with experimental information derived from diffraction data and Raman measurements.[162–164]

4.4 Vitreous Al_2O_3

The interest in the amorphous phase of Al_2O_3 has increased considerably in recent years because of the many important technological applications in catalysis,[165] luminescence[166] and optical devices.[167] Despite the vast number of studies on

alumina, many uncertainties remain and many contradicting results have been reported by both NMR experiments[168] and MD simulations.[169] For example, even though NMR is an experimental technique suited to perform local environment analysis, different ratios of coordination numbers for amorphous alumina (a-Al_2O_3) have been found.

The structural properties of models of vitreous Al_2O_3 at different densities, built by a simple and efficient stochastic quenching method, have recently been investigated by means of the GIPAW approach and compared to the α, θ, γ and κ crystalline phases[170] in order to solve the ambiguities of previous findings in the literature. The results have shown to be able to reproduce both XPS spectra and NMR chemical shifts. The set of calculated NMR chemical shifts reflects well resolved coordination environments for Al. The broadening of the NMR peaks due to local atomic environment differences in the amorphous phase has been estimated to be as large as 35 ppm. Therefore, the authors have drawn the conclusions that, in order to interpret the spectra correctly, an analysis of the details of the NMR spectra of amorphous alumina must consider differences in local environment for atoms with the same coordination number and Al–O distance. However, the authors in this paper did not compare the shape of theoretical NMR spectrum to the experimental one, but used instead the set of chemical shifts only. In this way, the quality of the overall structures could not be properly assessed.

5. Silicate glasses

5.1 Alkaline and alkaline-earth silicate glasses: random *vs* non-random cationic distributions

Although the effect of alkali and alkaline-earth cations on the depolymerization of the glass network has been clearly established,[171] the degree of disorder created by each mobile ion, the chemical and topological characteristics of its own local environment, and the mutual influence on the mobility of different ions (the so-called ''mixed alkali effect'') are still a matter for debate.[172,173] An important contribution to the understanding of alkali distribution has been given by the MD–GIPAW approach to alkaline and alkaline-earth silicate glasses with the compositions listed in Table 1.[17,85,174,175]

5.1.1 ^{29}Si NMR. *δ_{iso} peak maximum height*. The level of agreement between the theoretical and experimental ^{29}Si MAS NMR δ_{iso} of NS1, NS3, NS4, LS4 and CS glasses[17,85,174,175] has been utilized to judge the reliability of the three-dimensional models of these glasses (obtained either by a combined classical and *ab initio* MD approach or by classical MD followed by geometry optimization at the DFT level) to predict local environments for each investigated species (see Fig. 6). Further studies on the NMR response to atomic speciation carried out with the MD–GIPAW approach have revealed that especially well reproduced are (a) the strong increase in the ^{29}Si δ_{iso} values with alkali addition, indicating network depolymerization, (b) the maximum height of the peaks of each Q^n component of LS4, NS4 and CS glasses[17,175] (the difference shown between the theoretical data values and those derived by least-squares analysis of 1D and 2D ^{29}Si MAS NMR spectra[175,176] lies in the range 1–3 ppm) and (c) the 4 ppm difference between the maximum height of the peak of the Q^4 silicon atoms in NS4 and LS4 (NS4: Q^4 (theor.) = −103.2 ppm, Q^4 (sp.) = −105.5 ppm; LS4: Q^4 (theor.) = −107.2 ppm, Q^4 (sp.) = −109.2 ppm).[175]

Table 1 Glass compositions of the alkaline and earth-alkaline silicate glasses investigated with the MD–GIPAW approach

Glass	Composition (mol%)	Ref.s
NS1	$56.9SiO_2{\cdot}43.1Na_2O$	174
NS3	$77.5SiO_2{\cdot}22.5Na_2O$	174
NS4	$80.0SiO_2{\cdot}20.0Na_2O$	85,175
LS4	$80.0SiO_2{\cdot}20.0Li_2O$	175
CS	$50.0SiO_2{\cdot}50.0CaO$	17,94
NS	$75.0SiO_2{\cdot}25.0Na_2O$	94
CNS	$60.0SiO_2{\cdot}20.0Na_2O{\cdot}20.0CaO$	94
Mg_2SiO_4		178

Q^n distribution. Interestingly, a fair agreement has been found also between the Q^n contributions derived by the MD–GIPAW method and the empirical fitting of the experimental 1D ^{29}Si MAS NMR measurements of NS4 and LS4 (see Fig. 6). In the case of CS glass, the theoretical data are in very good agreement with the experimental 2D NMR measurements; the empirical fitting of the 1D MAS–NMR spectrum overestimates the more abundant Q^2 species by about 15% because of the intrinsic errors associated with the deconvolution procedure when, as in this case, the Q^n signal can hardly be approximated to a Gaussian function. It is worth noting that the core–shell potentials used by Pedone *et al.*[17] to derive the

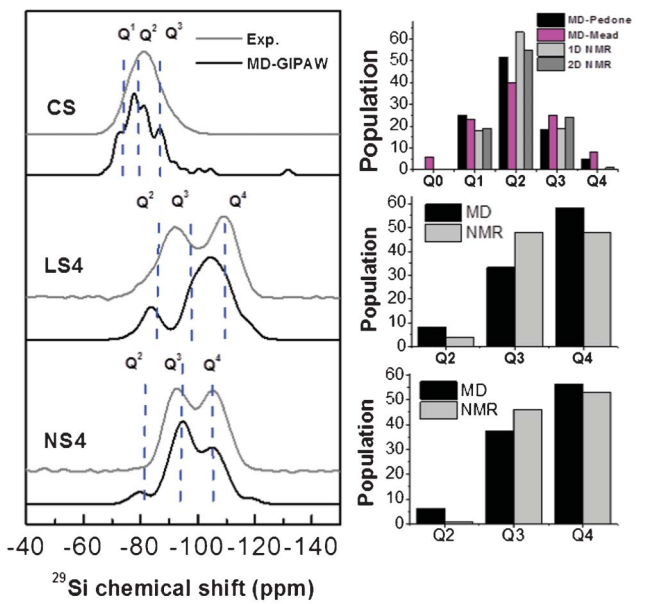

Fig. 6 Theoretical and experimental ^{29}Si MAS NMR spectra of NS4, LS4 and CS glasses (left). Q^n distributions of the three glasses obtained by means of MD simulations and NMR experiments (right). For the CS glass, MD–Pedone and MD–Mead stands for distributions obtained in ref. 17 and 117, respectively. 1D and 2D NMR are the distributions obtained by fitting the 1D and 2D NMR spectra by Zhang *et al.*[176]

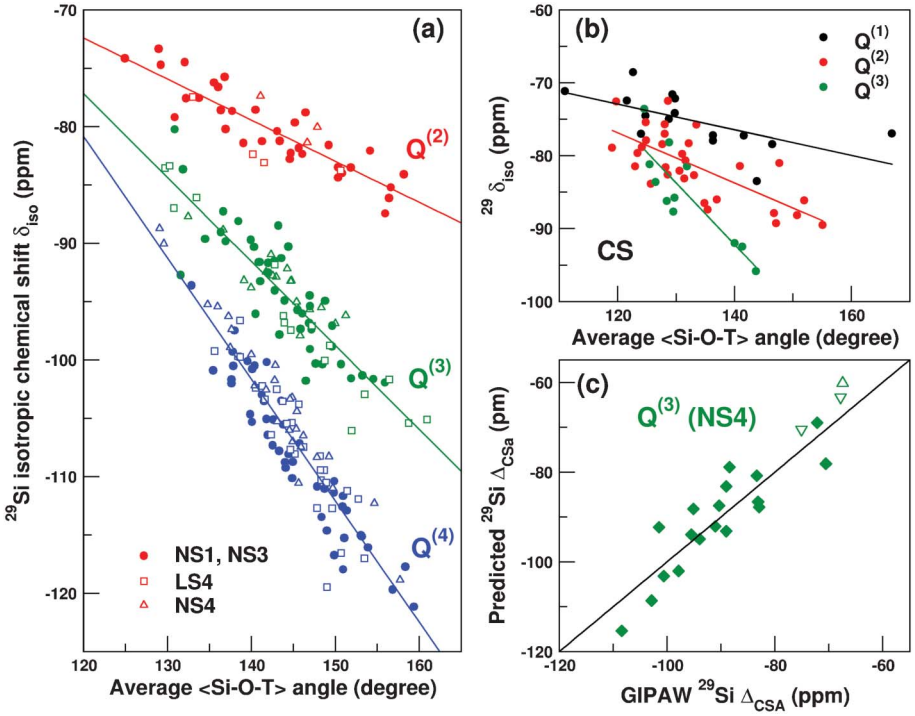

Fig. 7 Variation of the MD–GIPAW ^{29}Si isotropic chemical shifts as a function of the mean Si–O–Si bond angle for the different Q^n species in (a) NS1, NS3, NS4, LS4 and (b) CS glasses. (c) Calculated Q^3 ^{29}Si chemical shift anisotropy according to the empirical law $\Delta CS = -733.09 - 494.65 < Si + BO > + 938.18 < Si - NBO >$ (R = 0.879) *versus* (first principles) theoretical values. The solid line represents a perfect correspondence.

3D model of the CS glass furnish better results with respect to previous simulations that used the rigid ionic model and yielded a broader Q^n distribution.[177] Finally, a quantitative estimation of the degree of polymerization in near-stoichiometric Mg_2SiO_4 glass has been obtained by using the MD–GIPAW to interpret its ^{29}Si MAS NMR. The results are in favor of the presence of a large excess of bridging oxygen atoms associated with the $(Si_2O_7)^{6-}$ dimers.[178]

Quantitative structure–NMR parameters relationships. In agreement with previous results concerning both empirical relationships and theoretical approaches,[43,147,179–182] linear correlations between the Q^4, Q^3 and Q^2 isotropic chemical shifts (δ_{iso}) and the mean Si–O–T angle (where T denotes the Q^n connected tetrahedron) have been obtained for alkaline glasses (Fig. 7a) and a statistical model with accuracy in the δ_{iso} prediction of about 2 ppm as been established.[174] It is worth noting that the dependence of δ_{iso} upon Si–O–T is not affected by the nature of the modifier cations, (Na or Li in NS4 and LS4, respectively) since its variation can be described by the same regression for both glasses.[175]

Fig. 7b shows that worst correlations are obtained in the case of CS glass,[17] thus other structural parameters besides the mean Si–O–T angle could contribute to the ^{29}Si chemical shifts in the case of modifier ions like Ca. Poor correlations have also been recently noticed by Florian *et al.*[183] in the wollastonite system using a cluster approximation. This certainly has to be related to the covalent–ionic hybrid character of the Ca–O bonds.[86] This suggest that in order to obtain better correlations, models explicitly accounting for the Ca–O bond should be built. Unfortunately, the necessary NMR data (*i.e.* resolving the Si environment with respect to the Ca neighboring) are still difficult to acquire.

The mean value of the bond angle distribution can be estimated from the linear regressions obtained with an accuracy of 2–4°.[174] A mean Si–O–Si bond angle near 146° has been obtained for vitreous silica,[18] in line with the results of X-ray diffraction and absorption data which place the most probable angle for pure silica between 144°,[184] 147°[185] and 152°.[186] A downward shift is observed as the alkali concentration increases: 145° (LS4), 143° (NS4), 141.7° (NS3) and 133° (NS1).[174,175] Most importantly, from these correlations, direct information on different structural regions in glasses can be obtained since the mean values of the Si–O–T angles (T = Q^4, Q^3, Q^2) seen from different Q^n species is representative of polymerized and depolymerized regions. Multivariable regression analysis may represent a fruitful approach for future investigations, as shown by the bilinear correlation obtained for NS4 glass (Fig. 7c).[85] According to this equation, the chemical shift anisotropy Δ_{cs} of the Q^3 species can be predicted by the <Si–O>BO and <Si–O>NBO bond length, with errors less than 10 ppm.

5.1.2 ^{17}O NMR. A detailed description of the cation distribution around oxygen atoms has been reported recently for CS, NS and CSN glasses with the compositions reported in Table 1.[94] The increase in disorder generated by Ca around the oxygen atoms, with respect to that characteristic of Na, emphasized by the chemical disorder of cation mix in CSN, is reflected by the progressive increase in the widths of the

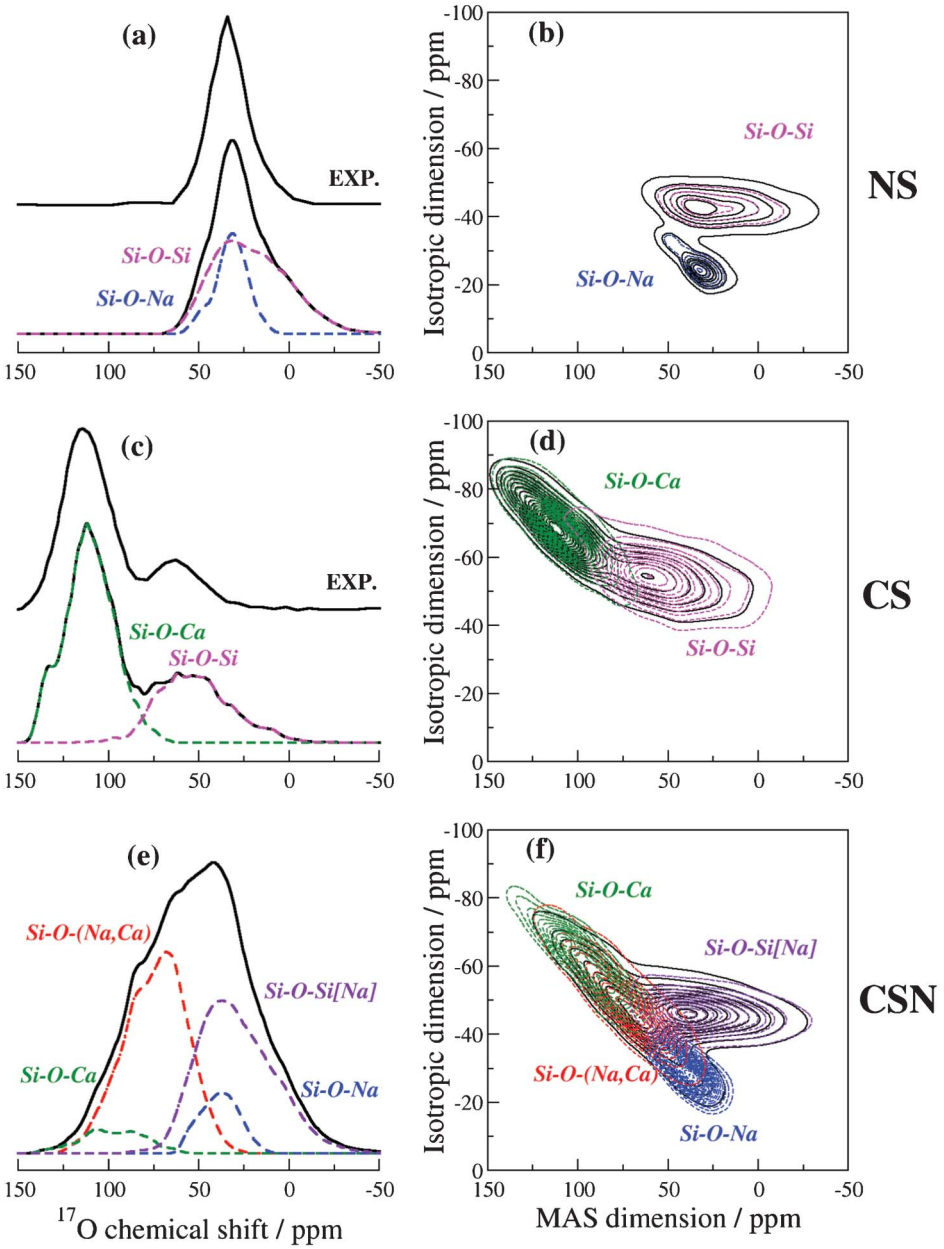

Fig. 8 Theoretical ^{17}O MAS and 3QMAS spectra of NS, CS and CSN glasses. The spectra of the different O sites are highlighted in colour. The experimental ^{17}O MAS spectra taken from literature are also reported for NS[49] and CS[239] glasses. Modifier cations surrounding BOs are reported in squared brackets while those surrounding NBOs in parenthesis. The figure is reprinted with permission from ref. 18 (refer for details), copyright 2012 American Chemical Society.

chemical shift distribution of NBO observed in both the ^{17}O MAS and 3QMAS spectra for NS, CS and CSN (Fig. 8). The signals of the Si–O–Na and Si–O–Si sites, overlapped in the ^{17}O MAS spectra, are well resolved in the theoretical 3QMAS spectra. Conversely, the Si–O–(Na,Ca) signals completely overlap with the Si–O–Ca and Si–O–Na ones in the ^{17}O 3QMAS spectrum of the CSN glass, therefore, a direct fitting of the experimental spectrum without the help of constraints derived from NMR calculations is not possible.

The analysis of the theoretical mean NMR parameters (δ_{iso}, C_Q, η_Q) and of the three-dimensional glass models have highlighted important information on the NBO and BO environments: (a) ^{17}O NMR signatures of BOs and NBOs continuously shift upon addition of sodium; fully polymerized regions, indicating the presence of zones rich in vitreous silica, are not observed in the spectrum of NS1 glasses; the limited overlap of the NS3-BO line with the SiO_2 ones have been attributed to the Q^4 species (37%) in NS3 glass; according to the three dimensional model of the glasses, the shift in the NMR parameters can be explained by a decrease of the Si–O–Si bond angle occurring when sodium atoms get closer to the oxygen atoms of the Si–O–Si linkage; a homogeneous distribution of Na around both oxygen species (BO and NBO) in the silicate network for these glass compositions is

envisaged.[174] (b) ^{17}O NMR δ_{iso} for NBO has shown to be sensitive to the nature of the cation in sodium and lithium silicate glasses (δ_{iso} = 52.4 ($\pm$12.7) ppm and 42.0($\pm$7.1) ppm for LS4 and NS4, respectively)[175] and to the number of Ca cations in the NBO surrounding (δ_{iso} = 118.3 ($\pm$12.8) ppm, 120.4 ($\pm$12.8) ppm, 123.6 ($\pm$16.6) ppm for CN_{Ca} = 2, 3, and 4, respectively).[17] This definitely elects δ_{iso} for NBO a valuable probe for evaluating the degree of cation mixing in mixed alkali glasses. Some relatively good correlations have been found between C_Q and η_Q values for BO and the geometrical parameters of the glasses.[17,175] In particular, a decrease of C_Q and an increase of η_Q is observed as a function of an increasing Si–O–Si bond angle. BO accommodates the presence of cations in its surroundings by decreasing its Si–O–Si bond angle, while increasing the Si–O distance for Na and Li glasses. The Si–O–Si angle variation is more pronounced for Na than for Li, despite the fact that Li cations are closer to the BO atom. (c) In CNS glass ^{17}O NMR δ_{iso} for NBO decreases with the number of Na cations around the oxygens, and increases with the amount of Ca cations, whereas the isotropic chemical shift of BOs increases with the number of Na or Ca ions within the first coordination sphere of the oxygens.[94] The most common environment around NBO and BO is represented by: Si–NBO(1Ca,2Na) 15.7%, Si–NBO(2Ca,1Na) 11.1%, Si–BO–Si[1Na] 20.4% and Si–BO–Si[2Na] 14.1% of sites. An extensive mixing of Ca and Na around NBO in soda–lime silicate glasses is observed, whereas BOs prefer to be surrounded by sodium ions rather than by calcium. The authors[94] ascribe the strong tendency for the formation of dissimilar cation pairs around NBOs to the very similar ionic radii of Ca and Na (the total amount of Si–NBO(Na,Ca) sites is 37.9%, while the NBOs coordinated to only Na or Ca species amount to 7.2 and 4.6%, respectively, of the total oxygen atoms present). However, the achievement of a homogeneous distribution of charges in the glass can also play an important role in the formation of dissimilar pairs.

5.1.3 ^{23}Na and ^{43}Ca NMR spectra. The ill-defined first coordination sphere of Na and Ca gives rise to ^{23}Na and ^{43}Ca MAS NMR broad enough to make a unique interpretation of the spectra difficult, therefore the MD–GIPAW approach has been mostly employed to investigate the trends of NMR parameters on the chemical environments of these ions.

Charpentier and coworkers[85,175] have recently highlighted clear trends between the ^{23}Na δ_{iso} data values and the number of coordinating NBO atoms to a given Na (positive slope), or mean Na–O bond length in NS1 and NS4 glasses (negative slope). They have showed that the ^{23}Na isotropic chemical shift can be predicted with errors less than 10 ppm as a mutilinear function of three structural parameters: the mean Na–O bond length, the number of coordinating bridging and non-bridging oxygens.[85] These correlations corroborate the influence of the bonding character of the coordinating oxygen atoms. Angeli *et al.*[174] have attributed the slight overestimation of ^{23}Na NMR C_Q observed for sodium in NS1 and NS3 glasses to thermal effects (motions and vibrations) which were not incorporated in their calculations. Gervais *et al.*[187] demonstrated that periodic DFT calculations can very accurately predict the ^{43}Ca NMR δ_{iso} of calcium in oxygen environments and well reproduce the relative values of the quadrupolar parameter, P_Q, provided that properly corrected Ca pseudopotential are employed. The ^{43}Ca δ_{iso} globally decreases as the average Ca–O bond distance increases, as experimentally observed by Angeli *et al.*[188] Pedone *et al.*[17] recently have demonstrated that the contribution of different sites of Ca cannot be resolved either with ^{43}Ca MAS or MQMAS (3Q, 5Q or 7Q) spectra. This severe limitation is overcome by the complementary information obtained with the ^{17}O probe (see above). Significant discrepancies are observed between the theoretical MQ NMR data reported in this study and the supposed distribution between different coordination environments suggested by Shimoda *et al.*[189] In fact, Pedone *et al.* have shown that the 7Q NMR spectra of Shimoda *et al.* can be very well simulated with a distribution rich in six-coordinated and poor in eight-coordinated calcium, derived by the MD simulations,[17,190] which differs from the suggestion of Shimoda *et al*.

6. Aluminosilicate glasses

When introducing Al_2O_3 in the fully connected corner-sharing tetrahedral network of amorphous silicates, the Al atoms substitute the Si atoms in the center of the tetrahedra thus leading to charged $(AlO_4)^-$ units, which are compensated by positive charges of cations, such as Na^+, K^+, Ca^{2+}, *etc.*, called charge-balance ions. For a total compensation of charges by the cations the system is fully polymerized (*e.g.* R = [CaO]/[Al_2O_3] = 1); if the concentration of cations becomes larger than what is needed for a full compensation of the $(AlO_4)^-$ units (for a ratio $R > 1$), the corner-sharing tetrahedral network brakes: some Si–O or Al–O bonds are replaced by weak M–O bonds and the cations are then called modifiers.[191] However, viscosity experiments[192] and high resolution 3QMAS NMR[193] have shown that this picture is not entirely correct for some aluminosilicate systems. Depolymerization of the network may occur even at R = 1 and the presence of NBO should be compensated by highly coordinated O sites, (*i.e.* O triclusters) to preserve the total number of Al–O and Si–O bonds. Yet, because of the lack of positional order, the experimental detection of such local structural units remains a challenging problem. Only very local probes such as X-ray absorption or NMR spectroscopies can help one to discriminate between the different structural units that might be present in very small proportions.[194] Moreover, in this framework, two distinct roles can be played by Ca^{2+} ions, namely as charge balancing non-bridging oxygens (NBO), or as charge compensating $(AlO_4)^-$ units. Very interesting questions arise on the overall arrangement of the 3D structure when there are additional elements in the system which can compete for such roles, such as sodium and magnesium.[190]

A contribution to the understanding of these open questions has been furnished recently by the MD–GIPAW approach to aluminosilicate glasses of composition 20.0 CaO 20.0Al_2O_3 60SiO_2 (CAS, all charge compensating framework charge),[93,194] 11Na_2O 11Al_2O_3 78SiO_2 (NAS, all charge balancing framework charge),[94] and 20CaO 10Na_2O 10Al_2O_3 60SiO_2 (CASN, both types of environment present).[94]

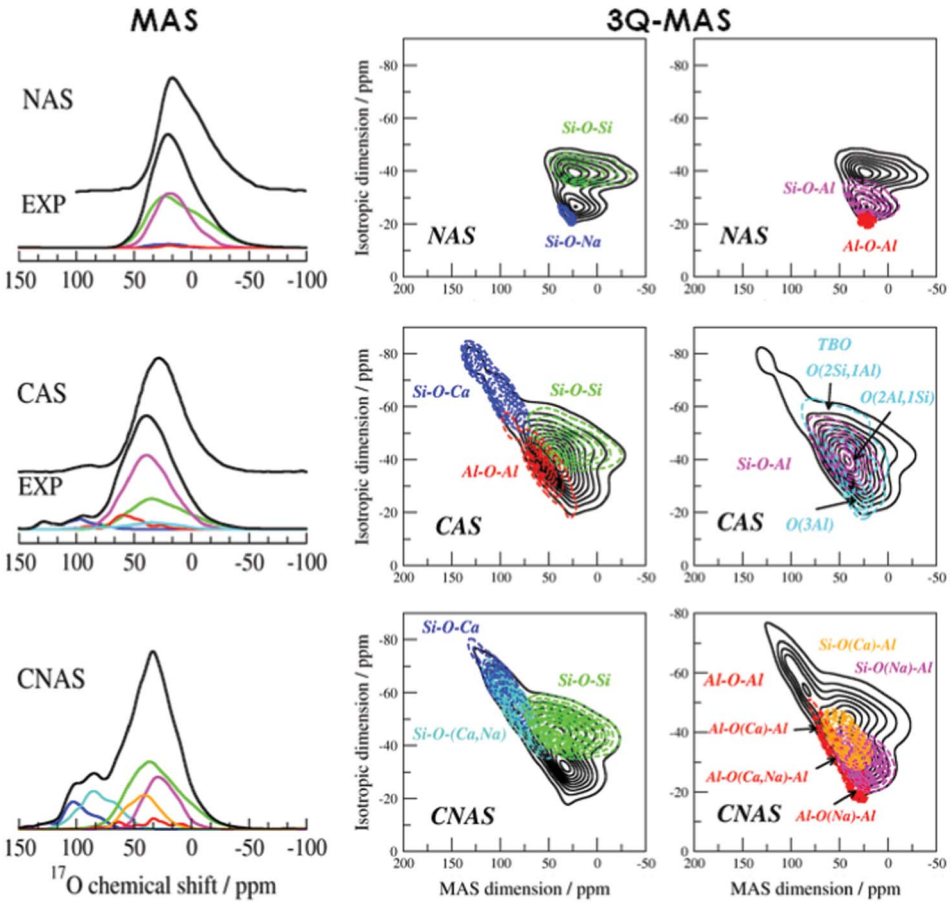

Fig. 9 Theoretical ^{17}O MAS NMR spectra at 14.1T for NAS, CAS and CNAS glasses (left). The spectra of the different O sites are highlighted in colour. The experimental ^{17}O MAS spectra taken from literature are also reported for NAS[195] and CAS[195] glasses. Theoretical ^{17}O 3QMAS NMR spectra at 14.1T for CAS, CNAS and NAS glasses (right). The spectra of the different O sites are highlighted in colour. The figure is reproduced from Pedone *et al.*[94] (with permission from ACS), to which refer for details. The figure is reprinted with permission from ref. 18 (refer for details), copyright 2012 American Chemical Society.

6.1 ^{17}O NMR

6.1.1 Intermixing of non-framework and framework cations. ^{17}O NMR proved to be a valuable probe for the investigation of the nature of non-framework cation mixing and the extent of intermixing among framework units in Na and Ca aluminosilicate glasses. The theoretical ^{17}O MAS NMR spectra of CAS, NAS and CASN glasses together with the contributions of the different oxygen speciations found in the MD-derived structural models have been compared in a recent work by Pedone *et al.*[94] Their results are summarized in Fig. 9 and 10. The overall shape of the spectra well reproduces the experimental ones for NAS[195] and CAS[193] glasses reported for validation purposes. A significant overlap among the Si–O–Si, Si–O–Al and Al–O–Al peaks in the ^{17}O MAS spectra makes it difficult to quantify the fractions of oxygen sites and explore the effect of composition on the topological disorder in the Si–O–Al sites from experiments alone. A better resolution is offered for NAS and CNAS glasses by the ^{17}O 3QMAS spectra, where all the multiple oxygen sites and the non-bridging oxygen peaks are distinguishable. For CAS glass the ^{17}O 3QMAS Si–O–Al spectrum is overlapped with those of Si–O–Si and Al–O–Al, therefore the agreement between the experimental assignments of the peaks in the 3QMAS spectra, reported by Stebbins,[193] and the one obtained by the computational analysis of the oxygen site populations[94] cannot be considered as obvious.

The small amount of Al–O–Al sites found in the investigated glasses reveals that the Al avoidance rule is not respected in amorphous solids, as also highlighted very recently by advanced ^{27}Al NMR experiments and molecular dynamics simulations on lanthanum aluminosilicate glasses.[79] The different types of BO and NBO sites surrounded by only Na cations, only Ca and mixed Na–Ca, occupy well-defined regions of the (δ_{iso}, C_Q) space and are distinguishable in the 3QMAS spectra as shown in Fig. 9.

From a detailed analysis of the CNAS structural models (Fig. 10) the authors[94] have observed that, similarly to soda–lime silicate glasses,[94] and in agreement with experimental evidence,[49,196] there is a non-random distribution of the network-modifying Ca and Na in soda–lime alluminosilicate glasses with the prevalence of dissimilar Na–Ca pairs around non-bridging NBOs (13.7% Si–NBO(Ca,Na)). However, in general, the NBOs are not coordinated by Na ions, which instead prefer to compensate the negative charge excess of the

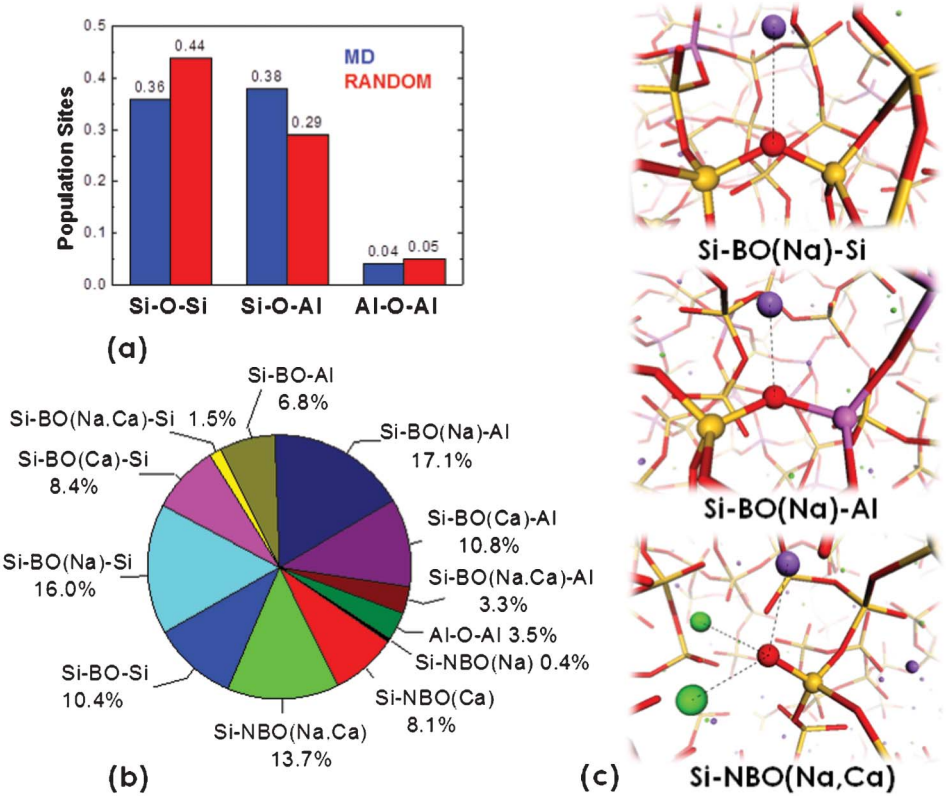

Fig. 10 (a) Histogram reporting the BO site populations of CNAS glasses derived from MD simulations and a random distribution of Al and Si connected to the central oxygen. (b) Pie chart reporting the BO and NBO site populations of CNAS glass derived from MD simulations. (c) Ball and Stick representations of Si–BO(Na)–Si, Si–BO(Na)–Al and Si–NBO(Na,Ca) sites found in the MD-derived CNAS structural models.

Si–O–Al sites (17.1%) or surround Si–BO–Si sites (16%). Moreover, an extensive mixing of framework units is observed in the CNAS glass, with the amount of Si–O–Al sites higher than that predicted by a random distribution. The Si–O–Al sites are surrounded by Na ions which play a preferential role as a charge-balancing cation, while Ca acts as a network-modifying cation.

6.1.2 Triclusters. The characterization of the TBOs in terms of NMR parameters is a difficult task because of both the small concentration of this species in the glass and of the overlap of the NMR parameters of the OAl_2Si and $OAlSi_2$ sites with those of the Si–O–Si and Si–O–Al sites in a 2D-3QMAS NMR ^{17}O spectrum.[194] Fig. 11 shows the local geometries of the tri-oxygen sites found in simulated glass structures of CAS glass. Only the NMR parameters of the OAl_3 triclusters, falling close to the edge of the main Si–O–Al peak, can be detected and their position in CAS glass[93,194] (see Fig. 9) is found to be in good agreement with experimental evidence.[193]

The OAl_3 sites are found in the CAS glass simulated by Pedone *et al.*[93] in two different structural motifs: (a) one Al atom as part of larger rings (C_Q value ranges between 2.6 and 3.5 MHz), (b) two Al atoms constitute a 2-membered Al_2O_2 ring (C_Q = 2.4 MHz). The small C_Q value characteristic of the 2-membered Al_2O_2 ring is consistent with the assignment of the *D* peak in the experimental 3QMAS spectra reported by Stebbins *et al.*[193] Therefore, the authors[93] have suggested that, if the *D* peak could be attributed to tricluster units, these must be of the OAl_3 type with Al embedded in small rings, although it must be noted that the calculated isotropic chemical shift of 40 ppm is much greater than that proposed by Stebbins *et al.*[193]

Finally, the comparison of CAS and NAS glasses shows that they contain 4.9 and 1.7% TBO, respectively. Thus, higher field strength cations promote the formation of NBO and TBO because of the competition for low-coordinate environments with respect to lower field strength cations. In fact, Ca prefers to be coordinated by NBO than by BO in its first coordination shell. Instead, all the NBOs present in the three glasses are associated with Si atoms rather than Al ones.

6.2 ^{27}Al NMR

The presence of TBO in the MD derived 3D structure of CAS glass has been interpreted by Pedone *et al.*[93] as the main reason for the inconsistencies observed between its theoretical and experimental ^{27}Al MAS NMR spectra (Fig. 12). In fact, notwithstanding the agreement found between the experimental and theoretical spectra for the maximum height of the peak (^{27}Al $\delta_{iso} \approx 50$ ppm, confirming a tetrahedral configuration of the aluminum atoms), the theoretical peak is larger than the experimental one and presents a shoulder at lower chemical shifts (40 ppm) that was not detected experimentally. Both these features can be ascribed to Al atoms connected to 1 TBO, which seems to be overestimated in the CAS models obtained both by classical[93] and Car–Parrinello MD simula-

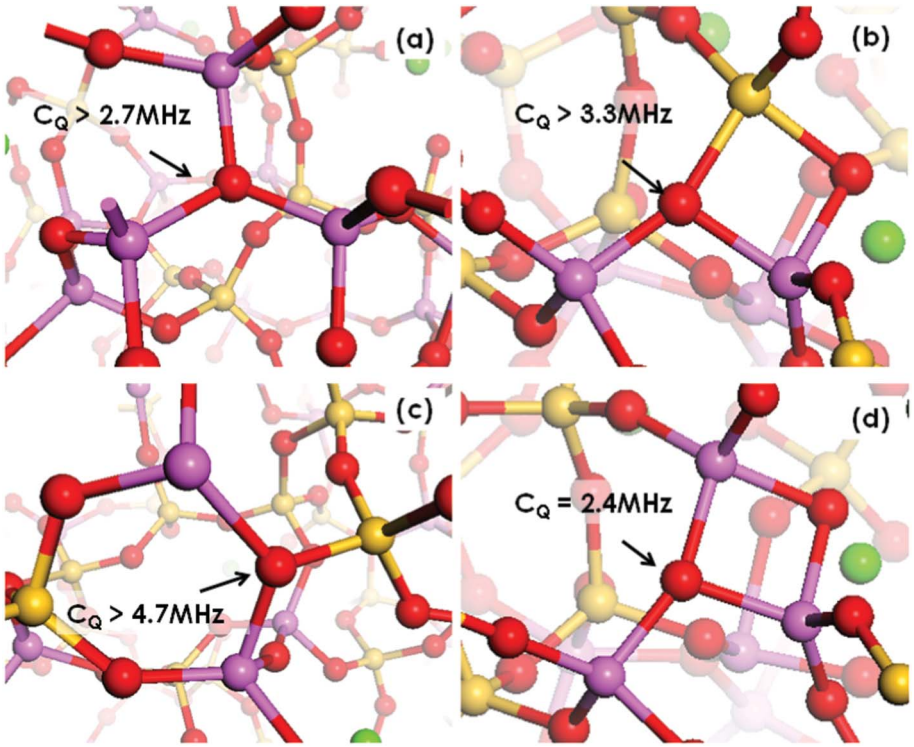

Fig. 11 Local geometry of oxygen tricluster sites found in simulated CAS glass. (a) OAl_3 sites in which Al is part of large rings. (b) OAl_2Si site in which one Al and the Si atom form a 2 membered ring. (c) OAl_2Si site in which Al and Si form large rings. (d) OAl_3 site in which Al is part of a 2-membered Al_2O_2 ring. Magenta, yellow and red spheres represent Al, Si and O atoms, respectively.

tions.[194] The presence of TBO leads to a non-ideal tetrahedral geometry around Al and increases the value of the quadrupolar coupling constant C_Q. As a consequence, the MAS NMR spectra are broader with the appearance of a double peak not detected experimentally. The detailed analysis of the second coordination sphere of Al ions shows that the medium-range order of the studied glass is governed by Q^4(4Si) (27%), Q^4(3Si,1Al) (40%) and Q^4(2Si,2Al) (22%) species. Both δ_{iso} and C_Q increase with the amount of Al ions in the second coordination sphere.

Finally, the classical MD 3D model contains two more defects: one fivefold coordinated Al ($Al^{[5]}$) with δ_{iso} = 10.7 ppm, and one threefold (Q^3) Al species with δ_{iso} = 62.9 ppm. The presence of penta-coordinated Al atoms in the real sample is clearly ruled out by the absence of the corresponding fingerprints; conversely, the signals coming from the Q^3 species could not be easily recognized from the experimental spectra since they fall in the same region as the Q^4 species. In light of these considerations, structural models arising from classical MD simulations might be only partially valid, but always efficient for the understanding of the NMR signature of the various Al environments.

6.3 Quantitative structure–NMR parameters relationships

Simple and accurate relationships between ^{17}O NMR parameters and local information such as Si–O distances and Si–O–T angles have not been found for the aluminosilicate glasses. Therefore, the generation of structural models of glasses and melts by means of MD simulations and the subsequent DFT–GIPAW calculations of the ^{17}O NMR parameters remains mandatory for an unambiguous interpretation of very complex multicomponent systems.[94]

As for the ^{27}Al NMR parameters, notwithstanding the poor correlation coefficient, an inverse relationship has been observed between the ^{27}Al δ_{iso} and Al–O–T bond angle,[93] thus confirming the results of previous experimental and theoretical studies.[61,197] The rationale behind the correlation between the shielding properties of Al atoms and the values of the Al–O–T angle has been unveiled by Liu *et al.*[198] in their *ab initio* NMR shielding calculations on model clusters. They demonstrated that the opening of the Al–O–T bond angle leads to a slight increase in the population of the Al–O and Si–O bond orbital electrons and a dramatic change in the bond orbital shapes and hybridization (with an increase in the s character and a decrease in bond bending). Moreover, the movement of one lone pair on the oxygen towards Al or Si contributes to the shielding of both Al and Si.

7. Bioglasses

The 45S5 Bioglass (46.1% SiO_2, 24.4% Na_2O, 26.9%CaO, 2.6% P_2O_5, in mol%), named hereafter BG, was the first material seen to form an interfacial bond with host tissue when implanted in rats.[199] Since then clinical uses of Bioglass particulates mainly concern periodontal and orthopedic applications. A crucial factor in the gene switching mechanism needed to initiate the required osteoblast activity is the rate at

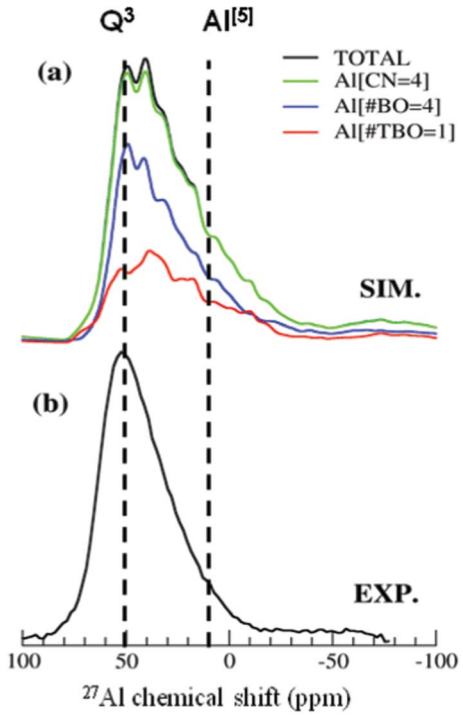

Fig. 12 (a) Simulated and (b) experimental ^{27}Al MAS spectra of CAS glass. The green line represents the spectrum of 4-fold coordinated Al ions without NBO connected to them, the blue line represents the spectrum of Al ions connected to 4 BO, while the red line represents the spectrum of Al ions connected to 1 TBO and 3 BO. The black dashed lines represent the peak position of Q^3 and 5-fold coordinated aluminum atoms (the latter gives rise to the tail at a higher chemical shift in the spectrum). The figure is reprinted with permission from ref. 93 (refer for details), copyright Springer 2012 Springer-Verlag.

which Ca, P and Si ions enter the fluid surrounding the glass.[200] This is strongly influenced by the concentration of phosphate units in the glass, which affects the silicon topological network, the environment of the Ca and Na sites and their distribution around oxygen ions.

The picture of the medium-range order of BG emerging from experimental and theoretical studies was initially characterized by a very open silicate network, mainly dominated by Q^2 Si and Q^3 Si interspersed with isolated orthophosphate groups. This simple binary model of the silica network, traditionally inferred from MAS NMR spectra,[201–205] has recently been demonstrated not to be optimal for the fitting of 1D MAS NMR spectra of bioactive glasses with variable concentration of phosphorus; therefore, a ternary model with Q^1, Q^2 and Q^3 Si species has been proposed,[31] in agreement with the results of Raman spectra[206] and of several classical and Car–Parrinello molecular dynamics simulations.[107,109,207,208] Moreover, recent ^{29}Si MAS NMR experiments,[31] IR and Raman data[206,209,210] and computational simulations[107,129,130,207,208] indicate that a small fraction of pyrophosphate (Q^1 or Si–O–P) species can coexist with the majority of orthophosphate species detected by earlier investigations.[201,202,204] The peak at 8 ppm in the ^{31}P MAS spectrum has indeed been assigned to pyrophosphate units by Angelopoulou *et al.*[205] in contradiction with other experimental interpretations[31,201,203] and computational studies.[92,131] This arrangement may strongly affect the phosphate release rate due to the labile nature of surface P–O–Si bridges.

New insights into this complex and contradictory description of the atomic level structure of 45S5 have been obtained by the application of the MD–GIPAW approach involving experimental and theoretical elaborations of solid state MAS ^{29}Si, ^{31}P, ^{23}Na, and ^{17}O and ^{23}Na 3QMAS NMR spectra.[20,92,131,211]

7.1 ^{29}Si NMR

From the results of a pioneering MD–GIPAW study by Pedone *et al.*[131] on BG, further evidence clearly emerges of the compatibility of a Q^n trinomial distribution with the experimental ^{29}Si NMR spectrum (see Fig. 13). In fact, the average values found for the peak maximum height of the ^{29}Si δ_{iso} theoretically derived (−79.0 ppm) compares well with the corresponding experimental one collected in the same paper (−78.0 ppm), and the average values of the peak maximum height of the Q^2 and Q^3 species theoretically derived are −79.5 and −87.0 ppm, in agreement with FitzGerald *et al.*,[201] whereas the average δ_{iso} of Q^1 species is −70.7 ppm, *i.e.* it lies in the −69.0 to −74.0 ppm range typical of silicate glasses.[212,213] Moreover, the Q^n distribution of the Si species is controlled by the non-random distribution of Na and Ca atoms in the glass. This can be inferred by the analysis of the correlation coefficients obtained for the linear correlations between the theoretical ^{29}Si δ_{iso} and the mean Si–O–T angle that yield R^2 of 0.55, 0.62 and 0.89 for Q^1, $Q^2$and Q^3 Si species, respectively. Differences in the correlations coefficients have to be ascribed to the number of Ca ions surrounding each Q^n species, as previously pointed out for the alkaline and alkaline-earth glasses (paragraph 5.1.1).[17] The lower the number of Ca ions, the higher the correlation coefficient, in fact the average number of Ca surrounding the Q^3 species is 1.6, with respect to 2.7, and 4.0 surrounding Q^2 and Q^1, the number of Na ions around the different Q^n Si sites being almost constant (4.4, 4.6 and 4.9 for Q^1, Q^2 and Q^1, respectively).

Another interesting point which has been addressed for bioactive glass doped with fluoride (FBG 46.2SiO_2, 24.3Na_2O, 16.9CaO, 10.0CaF_2, 2.6P_2O_5, in mol%)[92] is the potential presence of Si–F bonds detected in small amounts in the CP–MD three-dimensional model of the glass and in previous MD simulation studies.[214] The results obtained for the theoretical ^{29}Si MAS NMR parameters show a δ_{iso} shift of 6–11 ppm due to a Si–F bond. In particular, when an oxygen atom belonging to a Q^0 Si species is replaced by a fluorine atom the corresponding δ_{iso} decreases from −58.9 to −65.0 ppm (from −68.9 to −75.6 for a Q^1 Si species and from −78.0 to −88.9 for a Q^2 Si species) due to the increasing covalency of the Si–F bond. A significant increase of the chemical shift anisotropy is also observed, especially in the case of Q^0 Si species. Therefore, if present in the real glass, the Si–F species could be detectable by isotropic–anisotropic correlation 2D NMR spectra. Since neither 2D NMR nor ^{29}Si{^{19}F} REDOR experiments could detect this species with ^{29}Si in natural abundance, the authors have considered it a ''computational

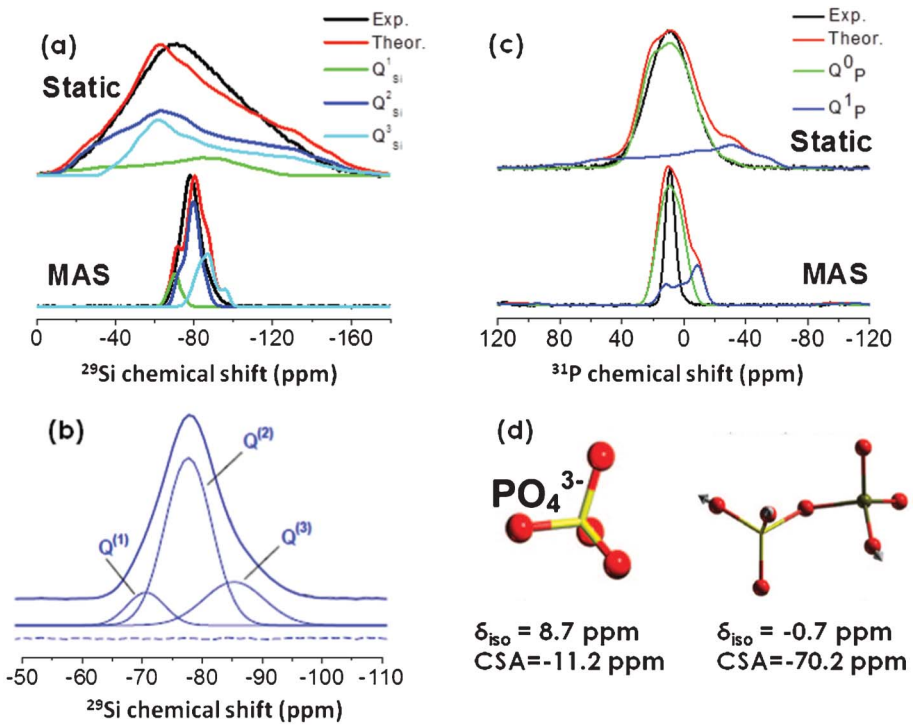

Fig. 13 (a) Comparison between experimental (black lines) and theoretical (colors) ^{29}Si static and MAS NMR spectra, at a magnetic field of 7.05 T. Individual spectra are scaled to the same maximum height. (b) Fit of the experimental ^{29}Si MAS NMR spectrum constrained by using an equation derived from compositional considerations (see ref. 131 for details). (c) Comparison between experimental (black lines) and theoretical static and MAS ^{31}P NMR spectra at a magnetic field of 7.05 T. (d) Representation of PO_4^{3-} and Si–O–P units with NMR parameters. The figures (a), (b) and (c) are reprinted with permission from ref. 131 (refer for details), copyright 2010 American Chemical Society.

defect'' that, since present in a negligible amount, does not invalidate the overall results as the NMR parameters of the other species (besides Si–F) are not affected (within the experimental precision of NMR experiments).

7.1.1 ^{31}P NMR. Following the same line of reasoning, the authors[92,131] have denoted an additional inaccuracy in the classical and CP–MD three-dimensional models of bioactive glasses, *i.e.* the presence of Si–O–P bridges. The Q^1 P signature would be very well distinguishable in both ^{31}P NMR and ^{17}O MQMAS experimental spectra, but is not observed in the experiments performed. Besides, the theoretical MAS and static ^{31}P NMR spectra reported in Fig. 13 show a peak characteristic of the Q^1 P species shielded by 9.4 ppm with respect to that of the Q^0, and a chemical shift anisotropy of the Q^1 P units (−70.2 ppm) much greater than the one calculated for Q^0 P units (−11.2 ppm). Therefore, the disagreement between the theoretical and the experimental spectra is obvious and indicates that the Si–O–P are a further ''computational defect'' due the high quenching rate and/or small size of the box used in the MD calculations.

Recently, a detailed structural characterization using ^{31}P multiple quantum NMR of a sodium free bioglass with a $46.1SiO_2$–$51.3CaO$–$2.6P_2O_5$ composition allowed for the first time to show directly nanometer-sized clusters of orthophosphates units, as well as Si–O–P bonds by using ^{29}Si–^{31}P dipolar experiments.[41] As such experiments are only based on dipolar interactions (which can be derived using geometrical parameters only) simulation of such NMR experiments from MD would be in principle feasible without having to resort to GIPAW calculations (but in the limit of the underlying ''pure'' NMR spin dynamics simulation, see ref. 215). Given the investigated scale length (several nm) this requires nevertheless the use of a large model.

7.1.2 ^{19}F NMR. Based on the theoretical ^{19}F MAS NMR results obtained for the most common fluorine units detected in the structural model of BF glass ($F[Ca_2Na_2]$, $F[Ca_2Na_3]$, $F[CaNa_3]$, $F[Ca_3Na]$ $[FCa_2Si]$ and $[FNa_2Si]$), Pedone *et al.*[92] have demonstrated that a precise deconvolution of the ^{19}F MAS NMR experimental spectra, by means of pure human-guided direct fitting, is very difficult and it could lead to misleading results because of the strong overlapping of the different signatures. In general the calculated spectra of the various F sites fall within the experimental isotropic chemical shift range and are important tools for the experimental spectra interpretation. However, it is worth noting that the three dimensional models obtained by MD simulations do not show any preference for F to be coordinated by Na or Ca, therefore the theoretical ^{19}F MAS NMR spectrum obtained by the MD–GIPAW approach does not reproduce the large band at −211 ppm of the experimental spectra characteristic of FNa_x clusters, that subtract sodium cations from the silicate network.

7.1.3 ^{87}Sr NMR. The question of the influence of Sr^{2+} on the structure and dissolution kinetics of bioglasses has been

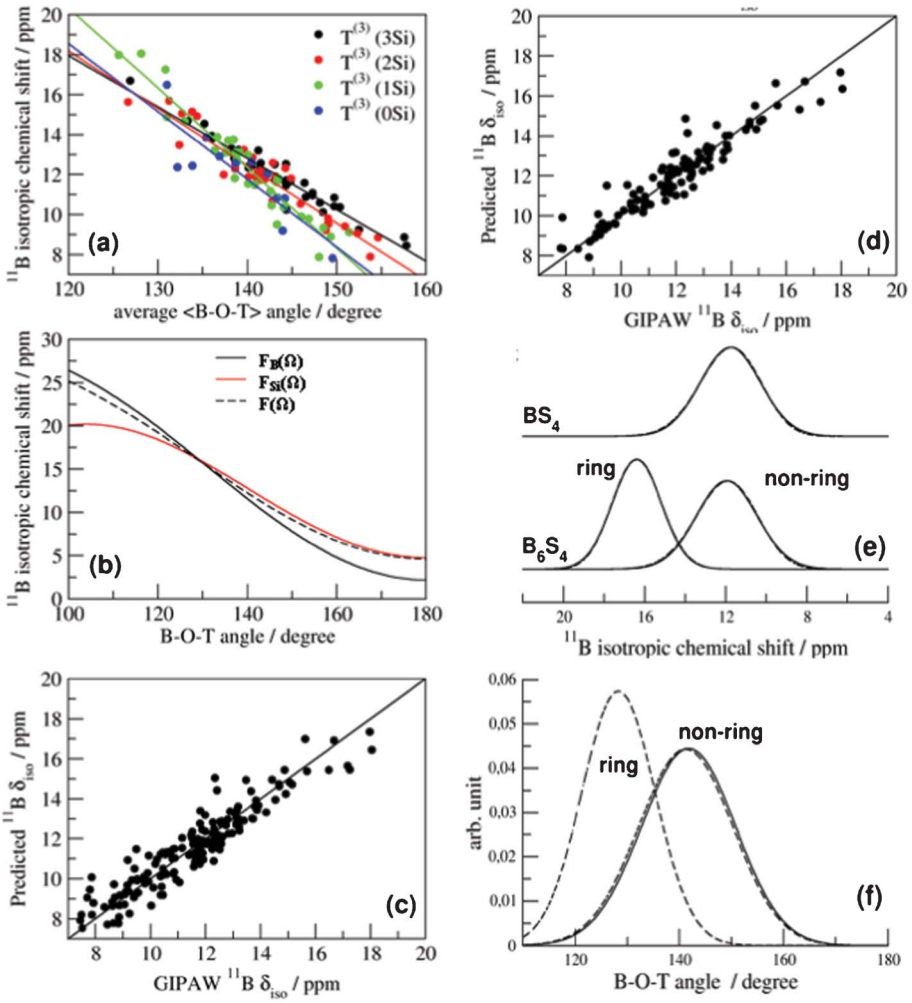

Fig. 14 (a) Theoretical ^{11}B GIPAW isotropic chemical shift δ_{iso} *versus* the average B–O–T bond angle (T = B, Si). In their paper, Soleilhavoup *et al.*[134] analyzed the relationship between δ_{iso} and the B–O–T (T B, Si) bond angles by using $\delta_{iso} = \frac{1}{3}\sum_{k=1}^{3} F(\Omega_k)$ (eqn (1)), where $F(\Omega)$ is a second order polynomial in cosΩ or by the relation $\delta_{iso} = \frac{1}{3}\sum_{k=1}^{3} F_{bk}(\Omega_k)$ (eqn (2)) in which the Si–O–B and B–O–B bridges have been considered to have different contributions defined by the functionals $F_{Si}(\Omega)$ and $F_B(\Omega)$, respectively.[134] (b) Plot of $F(\Omega)$, $F_B(\Omega)$ and $F_{Si}(\Omega)$ fitted on the ^{11}B δ_{iso} GIPAW calculations. Comparison between the predicted and GIPAW ^{11}B δ_{iso} using (c) eqn (1) and (d) eqn (2). (e) Experimental (as extracted from the fit of the ^{11}B MQMAS spectra, see Fig. 6 of ref. 134) and simulated isotropic chemical shift distributions calculated by using $p(\delta_{iso}) = \int d\Omega p(\Omega) \times \delta(\delta_{iso} - F(\Omega))$. (d) Predicted distribution of the B–O–T (T = B, Si) bond angle distribution extracted from the experimental isotropic chemical shift distribution by using $p(\Omega) = k \exp\left(\frac{\Omega - \bar{\Omega}}{2\sigma_\Omega^2}\right) \sin\Omega$.[134] The figure is reprinted with permission from ref. 134 (refer for details), copyright 2010 John Wiley & Sons, Ltd.

addressed by Bonhomme *et al.*[211] by implementing, within the MD–GIPAW approach, a new methodology to carry out ^{87}Sr NMR experiments on sol–gel prepared bioactive glasses before and after immersion in physiological fluids.

A model system based on the 76.9SiO_2–17.6CaO–5.5SrO mol% (B75–Sr10) composition was considered to study the sole influence of Sr on glass characteristics. This composition has been proved to be bioactive[216] and the effect of Sr in reducing the glass dissolution rate is more pronounced than with glasses of more complex compositions.[217] The authors[211] have used the results of MD–GIPAW calculations to determine *a priori* the set up of the ^{87}Sr experiments. The validity of the new methodology implemented has been demonstrated by the excellent agreement between the theoretical and experimental C_Q values for a set of several Sr-crystalline phases comprising structures characterized by very large C_Q constants such as for Sr-malonate, Sr-phenylphosphonate, α-SrP_2O_6, $SrSiO_3$ and $Sr_3(PO4)_2$. This is synthesized with a good correlation coefficient of the linear regression: C_Q (theoretical) = 0.929, C_Q (experimental) + 1.683, n = 10, R^2 = 0.987.

^{87}Sr GIPAW calculations for melt-and-quench models of Sr-glasses with various compositions in the SiO_2–CaO–SrO (such as B75–Sr10), SiO_2–SrO and SiO_2–Na_2O–CaO–SrO–P_2O_5 phase diagrams have been chosen to represent different strontium local environments. In fact, as the real sample B75–Sr10 (76.9SiO_2–17.6CaO–5.5SrO, mol%) was obtained by the sol–gel process (and not by a melt-and-quench synthetic procedure),

possible variations of composition corresponding to the partial phase separation of nanodomains were expected.

No clear trends relating quadrupolar parameters to local Sr environments have been established, thus corroborating the necessity of the MD–GIPAW approach to interpret complex ^{87}Sr NMR spectra. Interestingly, it has been found that the Sr silicate models are more similar to B75–Sr10 (from the ^{29}Si and ^{87}Sr NMR perspectives), which suggests that some phase segregation at the nanoscale may occur in the material. Such structural features, which had never been established previously, could be of importance, as they would provide new insight into the differences in reactivity of these materials.

8. Borosilicate glasses

The wide range of applications of borosilicate glasses and their use for high-level nuclear waste containment[218–220] or as bioactive systems[221] has triggered a great interest with respect to their structure–properties relationships. A recent paper by Soleilhavoup *et al.*[134] has focused on the extent of chemical disorder in binary borosilicate glasses and its influence on geometrical disorder.[222–225] The paper extends the MD–GIPAW methodology to extract structural distributions from NMR data, derived initially for vitreous silica, to three borosilicate glasses with B_2O_3–$5SiO_2$ (BS5) B_2O_3–$4SiO_2$ (BS4) and $6B_2O_3$–$4SiO_2$ (B6S4) formulae. In particular, (a) the distribution of NMR parameters, *i.e.* the distribution of isotropic chemical shifts for each boron resonance, is extracted from ^{11}B 3QMAS; (b) from MD–GIPAW calculations a quantitative relationship is established between the ^{11}B isotropic chemical shift and each B–O–B angle; (c) the NMR parameter distribution is mapped into a distribution of the B–O–B angle (structural inversion of the ^{11}B NMR spectrum), as shown in Fig. 14. For B-ring species, the distribution is bimodal because the two internal angles are highly constrained to a value close to 120° (indicative of nearly planar hexagonal rings), the third (external) angle describes the B(ring)–O–B(non-ring) linkages, assuming a mean value of 135.1° (±0.6°) with a standard deviation of 6.7° (±0.4°). A good agreement has been observed between these B–O–B data values and those derived by an alternative approach based on the analysis of ^{11}B MQDOR data to extract an accurate ^{11}B δ_{iso} distribution[226] and using a previous correlation determined from *ab initio* calculations on cluster models.[154,158] The structure of boroxol rings was characterized by 2 angles: an internal angle with a high constrain value of 120° and a free external angle (B(ring)–O–B(non-ring)). The latter was found to be around 141°–141.5° and rather independent of the glass composition. Comparison of the former mean value with the mean Si–O–T angle of 143.8°–145.0° obtained from ^{29}Si NMR suggests that boroxol rings are predominantly bonded to SiO_4 units in agreement with the prominent Si–O–B mixing observed in the ^{17}O NMR spectra.[222] It has been shown that, although the B–O–B angular distributions of the boroxol rings (and probably the Si–O–Si distributions) are not affected by temperature, a structural disorder is identified through the angular distributions of the bonds linking borate and silicate groups. This results in more broadly distributed BO_3 ring–O–(Si,B) and BO_3 non-ring–O–(Si,B) angles.[227]

9. Overcoming the limitations: new perspectives

If the MD–GIPAW has already proven to be a valuable tool to gain new insights into NMR data, there are still many perspectives for its improvement. NMR is constantly improving and many experiments such as heteronuclear or homonuclear correlations, dipolar recoupling to measure spatial proximity (for illustrative applications in Glasses see for example ref. 38,228–232) are close to be routinely applied. All these experiments involve NMR two-body interactions (dipolar or J coupling) so that multi spin-dynamics simulations[215,233,234] within MD–GIPAW will be required. It will offer the great advantage of providing reliable geometries and also permit an improved *in silico* numerical optimization of these experiments which can require several days of spectrometer time. Interestingly, as those experiments probe the glass structure at a longer scale, they will also provide new restraints for MD model assessment.

Inclusion of the dynamical effects has not yet been explored in the context of glassy materials. For ion conducting systems (which are of growing importance in the context of energy storage), full integrated methodologies will need to be built to correlate the calculated time dependency of NMR parameters to the experimental data, as already done in EPR.[235–237] With system sizes increasing (above 1000 atoms), it will be of interest to refine the model structures fitting the NMR spectra (*i.e.* as already done for structure factors using the refinement procedure).[29] This will however require efficiency gains in the computation of NMR shifts or in their accurate predictions with the help of semi-empirical models.[238] Larger systems will also offer the opportunity to address more complex chemical systems.

Acknowledgements

T.C. thanks the CCRT and the Grand Equipement National de Calcul Intensif (grant 096303) for access to HPC resources.

References

1 A. K. Varshneya, H. A. Schaeffer, H. A. Richardson, M. Wightman and L. D. Pye, *Processing, Properties, and Applications of Glass and Optical Materials*, Wiley, 2012.
2 E. El-Meliegy and R. van Noort, *Glasses and Glass Ceramics for Medical Applications*, Springer, London, 2012.
3 H. Eckert, Structural characterization of noncrystalline solids and glasses using solid-state NMR, *Prog. Nucl. Magn. Reson. Spectrosc.*, 1992, **24**, 159–293.
4 M. Eden, NMR studies of oxide-based glasses, *Annu. Rep. Prog. Chem., Sect. C*, 2012, **108**, 177–221.

5 D. Massiot, F. Fayon, V. Montouillout, N. Pellerin, J. Hiet, C. Roiland, P. Florian, J.-P. Coutures, L. Cormier and D. R. Neuville, Structure and dynamics of oxide melts and glasses: A view from multinuclear and high temperature NMR, *J. Non-Cryst. Solids*, 2008, **354**, 249–254.

6 S. K. Lee, Effect of pressure on structure of oxide glasses at high pressure: Insights from solid-state NMR of quadrupolar nuclides, *Solid State Nucl. Magn. Reson.*, 2010, **38**, 45–57.

7 J. F. Stebbins, P. Zhao, S. K. Lee and J. V. Oglesby, Direct observation of multiple oxygen sites in oxide glasses: recent advances from triple-quantum magic-angle spinning nuclear magnetic resonance, *J. Non-Cryst. Solids*, 2001, **293–295**, 67–73.

8 S. Kroeker, P. S. Neuhoff and J. F. Stebbins, Enhanced resolution and quantitation from 'ultrahigh' field NMR spectroscopy of glasses, *J. Non-Cryst. Solids*, 2001, **293–295**, 440–445.

9 C. J. Pickard and F. Mauri, All-electron magnetic response with pseudopotentials: NMR chemical shifts, *Phys. Rev. B: Condens. Matter*, 2001, **63**, 245101.

10 X. Xue and M. Kanzaki, NMR Characteristics of Possible Oxygen Sites in Aluminosilicate Glasses and Melts: An ab initio Study, *J. Phys. Chem. B*, 1999, **103**, 10816–10830.

11 X. Xue and M. Kanzaki, An ab initio calculation of ^{17}O and ^{29}Si NMR parameters for SiO_2 polymorphs, *Solid State Nucl. Magn. Reson.*, 2000, **16**, 245–259.

12 X. Xue and J. F. Stebbins, ^{23}Na NMR chemical shifts and the local Na coordination environments in silicate crystals, melts, and glasses, *Phys. Chem. Miner.*, 1993, **20**, 197–307.

13 X. Xue, J. F. Stebbins and M. Kanzaki, Correlations between ^{17}O NMR parameters and local structure around oxygen in high-pressure silicates and the structure of silicate melts at high pressure, *Am. Mineral*, 1994, **79**, 31–42.

14 X. Y. Xue and M. Kanzaki, Correlations between ^{29}Si, ^{17}O, and ^{1}H NMR properties and local structures in silicate: an ab initio calculation., *Phys. Chem. Miner.*, 1998, **26**, 14–30.

15 J. A. Tossell and P. Lazzeretti, Abinitio Calculations of Oxygen Nuclear-Quadrupole Coupling Constants and Oxygen and Silicon NMR Shielding Constants in Molecules Containing Si–O Bonds, *Chem. Phys.*, 1987, **112**, 205–212.

16 J. A. Tossell and P. Lazzeretti, Calculation of NMR Parameters for Bridgin Oxygens in $H_3Al–O–Al'H_3$, $H_3Si–O–Si'H_3$, $H_3P–O–P'H_3$ Linkages for Oxygen in SiH_3O^-. SiH_3OH and SiH_3OMg^+ and for Bridging Fluorine in $H_3SiFH_3^+$, *Phys. Chem. Miner.*, 1988, **15**, 564–569.

17 A. Pedone, T. Charpentier and M. C. Menziani, Multinuclear NMR of $CaSiO_3$ glass: simulation from first-principles, *Phys. Chem. Chem. Phys.*, 2010, **12**, 6054–6066.

18 T. Charpentier, P. Kroll and F. Mauri, First-Principles Nuclear Magnetic Resonance Structural Analysis of Vitreous Silica, *J. Phys. Chem. C*, 2009, **113**, 7917–7929.

19 T. Charpentier, The PAW/GIPAW approach for computing NMR parameters: A new dimension added to NMR study of solids, *Solid State Nucl. Magn. Reson.*, 2011, **40**, 1–20.

20 C. Bonhomme, C. Gervais, C. Babonneau, C. Coelho, F. Pourpoint, T. Axaïs, S. E. Ashbrook, J. M. Griffin, J. R. Yates, F. Mauri and C. J. Pickard, First-PrinciplesCalculation of NMR Parameters Using the Gauge Including Projector Augmented Wave Method: A Chemist's Point of View, *Chem. Rev.*, 2012, **112**, 5733–5779.

21 W. H. Zackariasen, The atomic arrangement in glass, *J. Am. Chem. Soc.*, 1932, **54**, 3841–3851.

22 J. S. Shelby, *Introduction to Glass and Technology*, The Royal Society of Chemistry, Cambridge, UK, 1997.

23 G. N. Greaves and S. Sen, Inorganic glasses, glass-forming liquids and amorphizing solids, *Adv. Phys.*, 2007, **56**, 1–166.

24 G. N. Greaves, EXAFS, glass structure and diffusion, *Philos. Mag. B*, 1989, **60**, 793–800.

25 G. N. Greaves and K. L. Ngai, Reconciling ionic-transport properties with atomic structure in oxide glasses, *Phys. Rev. B: Condens. Matter*, 1995, **52**, 6358–6380.

26 J. F. Stebbins, J. V. Oglesby and B. M. Lee, Oxygen sites in silicate glasses: a new view from oxygen-17 NMR, *Chem. Geol.*, 2001, **174**, 63–75.

27 S. K. Lee, Microscopic origins of macroscopic properties of silicate melts and glasses at ambient and high pressure: Implications for melt generation and dynamics, *Geochim. Cosmochim. Acta*, 2005, **69**, 3695–3710.

28 J. Gibson Murray, Solving amorphous structures-Two pairs beat one, *Science*, 2012, **335**, 929–930.

29 A. K. Soper, Partial structure factors from disordered materials diffraction data: An approach using empirical potential structure refinement, *Phys. Rev. B: Condens. Matter Mater. Phys.*, 2005, **72**, 104204.

30 E. Dupree and R. F. Pettifer, Determination of the Si–O–Si bond angle distribution in vitreous silica by magic angle spinning NMR, *Nature*, 1984, **308**, 523–525.

31 L. Linati, G. Lusvardi, G. Malavasi, L. Menabue, M. C. Menziani, P. Mustarelli, A. Pedone and U. Segre, Medium range order in phospho-silicate bioactive glasses: insights from MAS-NMR spectra, Chemical durability experiments and Molecular Dynamics Simulations, *J. Non-Cryst. Solids*, 2008, **354**, 84–89.

32 H. Maekawa, T. Maekawa, K. Kawamura and T. Yokokawa, The structural groups of alkali silicate-glasses determined from ^{29}Si MAS-NMR, *J. Non-Cryst. Solids*, 1991, **127**, 53–64.

33 U. Voigt, H. Lammert, H. Eckert and A. Heuer, Cation clustering in lithium silicate glasses: Quantitative description by solid-state NMR and molecular dynamics simulations, *Phys. Rev. B: Condens. Matter Mater. Phys.*, 2005, **72**, 64207.

34 L. Frydman and J. S. Harwood, Isotropic spectra of half-integer quadrupolar spins from bidimensional magic-angle spinning NMR, *J. Am. Chem. Soc.*, 1995, **117**, 5367–5368.

35 M. E. Smith and E. R. H. van Eck, Recent advances in experimental solid state NMR methodology for half-integer spin quadrupolar nuclei, *Prog. Nucl. Magn. Reson. Spectrosc.*, 1999, **34**, 159–201.

36 K. Mackenzie and M. E. Smith, *Multinuclear solid-state NMR of inorganic materials*, Pergamon, 2002.

37 S. E. Ashbrook, Recent advances in solid-state NMR spectroscopy of quadrupolar nuclei, *Phys. Chem. Chem. Phys.*, 2009, **11**, 6892–6905.

38 J. Hiet, M. Deschamps, N. Pellerin, F. Fayon and D. Massiot, Probing chemical disorder in glasses using silicon-29 NMR spectral editing, *Phys. Chem. Chem. Phys.*, 2009, **11**, 6935–6940.

39 M. Deschamps, F. Fayon, J. Hiet, G. Ferru, M. Derieppe, N. Pellerin and D. Massiot, Spin-counting NMR experiments for the spectral editing of structural motifs in solids, *Phys. Chem. Chem. Phys.*, 2008, **10**, 1298–1303.

40 D. Iuga, C. Morais, Z. Gan, D. R. Neuville, L. Cormier and D. Massiot, NMR Heteronuclear Correlation between Quadrupolar Nuclei in Solids, *J. Am. Chem. Soc.*, 2005, **127**, 11540–11541.

41 F. Fayon, C. Duée, T. Poumeyrol, M. Allix and D. Massiot, Evidence of Nanometric-Sized Phosphate Clusters in Bioactive Glasses as Revealed by Solid-State ^{31}P NMR, *J. Phys. Chem.*, **C**, 2013.

42 H. Eckert, S. Elbers, J. D. Epping, M. Janssen, M. Kalwei, W. Strojek and U. Voigt, Dipolar Solid State NMR Approaches Towards Medium-Range Structure in Oxide Glasses, *Top. Curr. Chem.*, 2004, **246**, 195–233.

43 M. Mägi, E. Lippmaa, A. Samoson and G. Engelhardt, Solid State High Resolution Silicon-29 Chemical Shifts in Silicates, *J. Phys. Chem.*, 1984, **88**, 1518–1522.

44 K. Mueller, J. H. Baltisberger, E. Wooten and A. Pines, Isotropic Chemical Shifts and Quadrupolar Parameters for Oxygen-17 using Dynamic-Angle Spinning NMR, *J. Phys. Chem.*, 1992, **96**, 7001–7004.

45 K. Mueller, Y. Wu, B. Chmelka, J. F. Stebbins and A. Pines, High-resolution oxygen-17 NMR of solid silicates, *J. Am. Chem. Soc.*, 1990, **113**, 32–38.

46 H. Koller, G. Engelhardt, A. P. M. Kentgens and J. Sauer, ^{23}Na NMR Spectroscopy of solids: interpretation of quadrupole interaction parameters and chemical shifts, *J. Phys. Chem.*, 1994, **98**, 1544–1551.

47 A. M. George and J. F. Stebbins, High temperature ^{23}Na NMR data for albite: comparison to chemical shift models, *Am. Mineral*, 1995, **80**, 878–884.

48 J. F. Stebbins, Cation sites in mixed-alkali oxide glasses: correlations of NMR chemical shift data with site size and bond distance, *Solid State Ionics*, 1998, **112**, 137–141.

49 S. K. Lee and J. F. Stebbins, Nature of Cation Mixing and Ordering in Na-Ca Silicate Glasses and Melts, *J. Phys. Chem. B*, 2003, **107**, 3141–3148.

50 E. Lippmaa, A. Samoson and M. Magi, High resolution aluminum-27 NMR of aluminosilicates, *J. Am. Chem. Soc.*, 1986, **108**, 1730–1735.

51 G. Engelhardt, *High-resolution solid state NMR of silicates and zeolites*, Wiley, Chichester, 1987.

52 S. Kroeker and J. F. Stebbins, Three-coordinate boron-11 chemical shifts in borates, *Inorg. Chem.*, 2001, **40**, 6239–6246.

53 B. Zhou, V. K. Michaelis, S. R. Giesbrecht, S. Kroeker, B. L. Sherriff, Z. Sun, Y. F. Yao and Y. Pan, Correlations between ^{11}B NMR parameters and structural characters in borate and borosilicate minerals investigated by high-resolution MAS NMR and ab initio calculations, *Phys. Chem. Miner.*, 2012, **39**, 363–372.

54 J. A. Tossell, Calculation of NMR Shieldings and other Properties for 3 and 5 coordinate Si, 3 coordinate-O and some Siloxane and Boroxol Ring Compounds, *J. Non-Cryst. Solids*, 1990, **120**, 13–19.

55 C. Lindsay and J. A. Tossell, Ab initio Calculations of ^{17}O and (N)T NMR Parameters (N) T = ^{31}P, ^{29}Si) in H_3TOTH_3 dimers and T_3O_9 Trimeric rings, *Phys. Chem. Miner.*, 1991, **18**, 19110–19113.

56 U. Sternberg, The bond angle dependence of the asymmetry parameter of the oxygen-17 electric field gradient tensor, *Solid State Nucl. Magn. Reson.*, 1993, **2**, 181–190.

57 P. J. Grandinetti, J. H. F. Baltisberger, I. J. F. Stebbins, H.-J. Werner and A. Pines, Solid-state ^{17}O Magic-angle and dynamic-angle spinning NMR study of the SiO_2 polymorph coesite, *J. Phys. Chem.*, 1995, **99**, 12341–12348.

58 T. Clark, P. J. Grandinetti, P. Florian and J. F. Stebbins, An ^{17}O NMR investigation of crystalline sodium metasilicate: implications for the determination of local structure in alkali silicates, *J. Phys. Chem.*, 2001, **105**, 12257–12265.

59 H. Maekawa, P. Florian, D. Massiot, H. Kiyono and M. Nakaruma, Effect of alkali metal oxide on ^{17}O NMR parameters and Si–O–Si angles of alkali metal disilicate glasses, *J. Phys. Chem.*, 1996, **100**, 5525–5532.

60 J. A. Tossell, Quantum mechanical calculation of ^{23}Na NMR shieldings in silicates and aluminosilicates, *Phys. Chem. Miner.*, 1999, **27**, 70–80.

61 I. Farnan, P. J. Grandinetti, J. H. Baltisberger, J. F. Stebbins, U. Werner, M. A. Eastman and A. Pines, Quantification of disorder in network-modified silicate glasses, *Nature*, 1992, **358**, 31–35.

62 F. Angeli, J.-M. Delaye, T. Charpentier, J.-C. Petit, D. Ghaleb and P. Faucon, Influence of glass chemical composition on the Na-O bond distance: a ^{23}Na 3Q-MAS NMR and molecular dynamics study, *J. Non-Cryst. Solids*, 2000, **276**, 132–144.

63 F. Angeli, J.-M. Delaye, T. Charpentier, J.-C. Petit, D. Ghaleb and P. Faucon, Investigation of Al–O–Si bond angle in glass by ^{27}Al 3Q-MAS NMR and molecular dynamics, *Chem. Phys. Lett.*, 2000, **320**, 681–687.

64 J. A. Tossell and J. Horbach, O triclusters revisited: classical MD and quantum cluster results for glasses of composition $(Al_2O_3)2(SiO_2)$, *J. Phys. Chem. B*, 2005, **109**, 1794–1797.

65 A. Pedone, M. Biczysko and V. Barone, Environmental Effects in Computational Spectroscopy, *ChemPhysChem*, 2010, **11**, 1812–1832.

66 A. Pedone, M. Pavone, M. C. Menziani and V. Barone, Accurate First-Principle Prediction of ^{29}Si and ^{17}O NMR Parameters in SiO_2 Polymorphs: The Cases of Zeolites Sigma-2 and Ferrierite, *J. Chem. Theory Comput.*, 2008, **4**, 2130–2140.

67 J. Casanovas, F. Illas and G. Pacchioni, Ab initio calculations of ^{29}Si solid state NMR chemical shifts of silcane and silanol groups in silica, *Chem. Phys. Lett.*, 2000, **326**, 523–529.

68 S. Cadars, D. H. Brouwer and B. F. Chmelka, Probing local structures of siliceous zeolite frameworks by solid-state NMR and first-rpinciples calculations of ^{29}Si–O–^{29}Si scalar couplings, *Phys. Chem. Chem. Phys.*, 2009, **11**, 1825–1837.

69 J. D. Kubicki and M. J. Toplis, Molecular orbital calculations on aluminosilicate tricluster molecules, *Am. Mineral*, 2002, **87**, 668–678.

70 J. D. Kubicki and B. D. Sykes, Ab initio calculation of ^{1}H, ^{17}O, ^{27}Al and ^{29}Si NMR parameters, vibrational frequen-

cies and bonding energetics in hydrous silica and Na-aluminosilicate glasses, *Geochim. Cosmochim. Acta*, **68, 68**, 3909–3918.

71 L. Olivier, X. Yuan, A. N. Cormack and C. Jäger, Combined 29Si double quantum NMR and MD simulation studies of network connectivities of binary $Na_2O{\cdot}SiO_2$ glasses: new prospects and problems, *J. Non-Cryst. Solids*, 2001, **293–295**, 53–66.

72 C. Leonelli, G. Lusvardi, M. Montorsi, M. C. Menziani, L. Menabue, P. Mustarelli and L. Linati, Influence of small additions of Al_2O_3 on the properties of the $Na_2O{\cdot}3SiO_2$ glass, *J. Phys. Chem. B*, 2001, **105**, 919–927.

73 B. Park, H. Li and L. R. Corrales, Molecular dynamics simulation of La_2O_3–Na_2O–SiO_2 glasses. II. The clustering of La^{3+} cations, *J. Non-Cryst. Solids*, 2002, **297**, 220–238.

74 L. Barbieri, V. Cannillo, C. Leonelli, M. Montorsi, C. Siligardi and P. Mustarelli, Characterisation of CaO–ZrO_2–SiO_2 glasses by MAS-NMR and molecular dynamics, *Phys. Chem. Glasses-B*, 2004, **45**, 138–140.

75 E. Kashchieva, B. Shivachev and Y. Dimitriev, Molecular dynamics studies of vitreous boron oxide, *J. Non-Cryst. Solids*, 2005, **351**, 1158–1161.

76 J. Machacek, O. Gedeon and M. Liska, Molecular approach to the 5-coordinated silicon atoms in silicate glasses, *Phys. Chem. Glasses*, 2007, **48**, 345–353.

77 J. Machacek, O. Gedeon and M. Liska, Group connectivity in binary silicate glasses, *J. Non-Cryst. Solids*, 2006, **352**, 2173–2179.

78 G. Mountjoy, B. M. Al-Hasni and C. Storey, Structural organisation in oxide glasses from molecular dynamics modeling, *J. Non-Cryst. Solids*, 2011, **357**, 2522–2529.

79 A. Jaworski, B. Stevensson, B. Pahari, K. Okhotnikov and M. Eden, Local Structures and Al/Si Ordering in Lanthanum Aluminosilicate Glasses Explored by Advanced ^{27}Al NMR Experiments and Molecular Dynamics Simulations, *Phys. Chem. Chem. Phys.*, 2012, **14**, 15866–15878.

80 H. Inoue, A. Masuno and T. Watanabe, Modeling of the structure of sodium borosilicate glasses using pair potentials, *J. Phys. Chem. B*, 2012, **116**, 12325–12331.

81 L. L. Linati, G. Malavasi, G. Menabue, L. Menziani, M. C. Mustarelli and P. U. Segre, Qualitative and quantitative Structure-Property Relationships (QSPR) analysis of multi-component potential bioglasses, *J. Phys. Chem. B*, 2005, **109**, 4989–4998.

82 G. Malavasi, A. Pedone and M. C. Menziani, Towards a quantitative rationalization of multicomponent glass properties by means of Molecular Dynamics Simulations, *Mol. Simul.*, 2006, **32**, 1045–1055.

83 M. Profeta, F. Mauri and C. J. Pickard, Accurate First Principles Prediction of ^{17}O NMR Parameters in SiO_2: Assignment of Zeolite Ferrierite Spectrum, *J. Am. Chem. Soc.*, 2003, **125**, 541–548.

84 J. R. Yates, C. J. Pickard and F. Mauri, Calculation of NMR chemical shifts for extended systems using ultrasoft pseudopotentials, *Phys. Rev. B: Condens. Matter Mater. Phys.*, 2007, **76**, 024401–024411.

85 T. Charpentier, S. Ispas, M. Profeta, F. Mauri and C. J. Pickard, First-principles calculation of ^{17}O, ^{29}Si, and ^{23}Na NMR spectra of sodium silicate crystals, *J. Phys. Chem. B*, 2004, **108**, 4147–4161.

86 M. Profeta, M. Benoit, F. Mauri and C. J. Pickard, First-Principles Calculation of the ^{17}O NMR Parameters in Ca Oxide and Ca Aluminosilicates: the Partially Covalent Nature of the Ca–O Bond, a Challenge for Density Functional Theory, *J. Am. Chem. Soc.*, 2004, **126**, 12628–12635.

87 F. Tielens, C. Gervais, J. F. Lambert, F. Mauri and D. Costa, Ab Initio Study of the Hydroxylated Surface of Amorphous Silica: a New Model, *Chem. Mater.*, 2008, **20**, 3336–3344.

88 G. Ferlat, T. Charpentier, A. P. Seitsonen, A. Takada, M. Lazzeri, L. Cormier, G. Calas and F. Mauri, Boroxol Rings in Liquid and Vitreous B_2O_3 from First Principles, *Phys. Rev. Lett.*, 2008, **101**, 065504.

89 J. V. Hanna, K. J. Pike, T. Charpentier, T. F. Kemp, M. E. Smith, B. E. G. Lucier, R. W. Schurko and L. S. Cahill, A ^{93}Nb Solid-State NMR and Density Functional Theory Study of Four- and Six-Coordinate Niobate Systems, *Chem.–Eur. J.*, 2010, **16**, 3222–3239.

90 P. Florian, E. Veron, T. F. G. Green, J. R. Yates and D. Massiot, Elucidation of the Al/Si Ordering in Gehlenite $Ca_2Al_2SiO_7$ by Combined ^{29}Si and ^{27}Al NMR Spectroscopy/Quantum Chemical Calculations, *Chem. Mater.*, 2012, **24**, 4068–4079.

91 S. W. Reader, M. R. Mitchell, K. E. Johnston, C. J. Pickard, K. R. Whittle and S. E. Ashbrook, Cation Disorder in Pyrochlore Ceramics: ^{89}Y MAS NMR and First-Principles Calculations, *J. Phys. Chem. C*, 2009, **113**, 18874–18883.

92 A. Pedone, T. Charpentier and M. C. Menziani, The Structure of Fluoride-containing Bioactive Glasses: new insights from First-Principles Calculations and Solid State NMR Spectroscopy, *J. Mater. Chem.*, 2012, **22**, 12599–12608.

93 A. Pedone, E. Gambuzzi, G. Malavasi and M. C. Menziani, First-Principles Simulations of the ^{27}Al and ^{17}O Solid State NMR spectra of a calcium alumino-silicate glass, *Theor. Chem. Acc.*, 2012, **131**, 1147–1157.

94 A. Pedone, E. Gambuzzi and M. C. Menziani, Unambiguous Description of the Oxygen Environment in Multicomponent Aluminosilicate Glasses from ^{17}O Solid State NMR Computational Spectroscopy, *J. Phys. Chem. C*, 2012, **115**, 14599–14609.

95 E. Balan, F. Mauri, C. J. Pickard, I. Farnan and G. Calas, The aperiodic states of zircon: an ab initio molecular dynamics study, *Am. Mineral*, 2003, **88**, 1769–1777.

96 M. Kibalchenko, J. R. Yates, C. Massobrio and A. Pasquarello, Structural Composition of First-Neighbor Shells in $GeSe_2$ abd $GeSe_4$ Glasses from First-Principles Analyss of NMR Chemical Shifts, *J. Phys. Chem. C*, 2011, **115**, 7755–7759.

97 M. Kibalchenko, J. R. Yates, C. Massobrio and A. Pasquarello, Structural Assegniments of NMR chemical shifts in Ge_xSe_{1-x} glasses via first-principles calculations for $GeSe_2$, Ge_4Se_9 and GeSe crystals, *Phys. Rev. B: Condens. Matter Mater. Phys.*, 2010, **82**, 020202.

98 M. Bak, J. T. Rasmussen and N. C. Nielsen, SIMPSON: A general simulation program for solid-state NMR spectroscopy, *J. Magn. Reson.*, 2001, **147**, 296–330.

99 Z. H. Gan, Isotropic NMR spectra of half-integer quadrupolar nuclei using satellite transitions and magic-angle spinning, *J. Am. Chem. Soc.*, 2000, **122**, 3242–3243.

100 J. Mahler and A. Sebald, Deconvolution of ^{29}Si MAS NMR spectra of silicate glasses revisited-some critical comments, *Solid State Nucl. Magn. Reson.*, 1995, **5**, 63.

101 M. P. Allen and D. J. Tidesley, *Computer simulation of liquids*, Oxford Science Publication, Oxford, 1987.

102 A. Pedone, Properties Calculations of Silica-Based Glasses by Atomistic Simulations Techniques: A Review, *J. Phys. Chem. C*, 2009, **113**, 20773–20784.

103 M. Pota, A. Pedone, G. Malavasi, C. Durante, M. Cocchi and M. C. Menziani, Molecular Dynamics Simulations of Sodium Silicate Glasses: Optimization and Limits of the Computational Procedure, *Comput. Mater. Sci.*, 2010, **47**, 739–751.

104 A. Pedone, G. Malavasi, M. C. Menziani, A. N. Cormack and U. Segre, A New Self-Consistent Empirical Interatomic Potential Model for Oxides, Silicates, and Silica Based Glasses, *J. Phys. Chem. B*, 2006, **110**, 11780–11795.

105 M. Salanne, B. Rotenberg, S. Jahn, R. Vuilleumier, C. Simon and P. A. Madden, Including many-body effects in models for ionic liquids, *Theor. Chem. Acc.*, 2012, **131**, 1143–1149.

106 G. Dick and A. W. Overhauser, Theory of the Dielectric Constants of alkali Halide Crystals, *Phys. Rev.*, 1958, **112**, 90–103.

107 A. Tilocca, Short- and medium-range structure of multicomponent bioactive glasses and melts: An assessment of the performances of shell-model and rigid-ion potentials, *J. Chem. Phys.*, 2008, **129**, 084504.

108 A. Tilocca, N. de Leeuw and A. N. Cormack, Shell-model molecular dynamics calculations of modified silicate glasses, *Phys. Rev. B: Condens. Matter Mater. Phys.*, 2006, **73**, 104209–104223.

109 A. Pedone, G. Malavasi and M. C. Menziani, Computational Insight Into the Effect of CaO/MgO Substitutions on the Structural Properties of Phosphosilicate Bioactive Glasses, *J. Phys. Chem. C*, 2009, **113**, 15723–15730.

110 H. Yu and W. F. van Gunsteren, Accounting for polarization in molecular simulations, *Comput. Phys. Commun.*, 2005, **172**, 69–85.

111 B. P. Feuston and S. H. Garofalini, Empirical three-body potential for vitreous silica, *J. Chem. Phys.*, 1988, **89**, 5818–5825.

112 B. W. H. van Beest, G. J. Kramer and R. A. van Santen, Force fields for silicas and aluminophosphates based on ab initio calculations, *Phys. Rev. Lett.*, 1990, 64.

113 A. Pedone, G. Malavasi, M. C. Menziani, U. Segre, F. Musso, M. Corno, B. Civalleri and P. Ugliengo, FFSiOH: a new Force Fields for Silica Polymorphs and their Hydroxylated Surfaces based on Periodic B3LYP calculations, *Chem. Mater.*, 2008, **20**, 2522.

114 E. Chagarov, J. B. Adams and J. Kieffer, Application of Design of Experiments Methodology to Optimization of Classical Molecular Dynamics Generation of Amorphous SiO_2 Structure, *Modell. Simul. Mater. Sci. Eng.*, 2004, **12**, 337.

115 B. M. Lee, H. K. Baik, B. S. Seong, S. Munetoh and T. Motooka, Generation of glass SiO_2 structures by various cooling rates: A molecular-dynamics study, *Comput. Mater. Sci.*, 2006, **37**, 203–208.

116 L. R. Corrales and J. Du, Thermal kinetics of glass simulations, *Phys. Chem. Glasses*, 2005, **46**, 420–424.

117 K. Vollmayer, W. Kob and K. Binder, Cooling Rate Effects in Amorphous Silica: A Computer Simulation, *Phys. Rev. B: Condens. Matter*, 1996, **54**, 15808–15827.

118 A. N. Cormack and J. Du, Molecular dynamics simulations of soda-lime-silicate glasses, *J. Non-Cryst. Solids*, 2001, **293–295**, 283–289.

119 L. Adkins and A. N. Cormack, Large-scale simulations of sodium silicate glasses, *J. Non-Cryst. Solids*, 2011, **357**, 2538–2541.

120 M. C. Payne, M. P. Teter, D. C. Allan, T. A. Arias and J. D. Joannopulos, Iterative minimization techniques for ab initio total-energy calculations: molecular dynamics and conjugate gradients, *Rev. Mod. Phys.*, 1992, **64**, 1045–1097.

121 R. Car and M. Parrinello, Unified approach for molecular dynamics and density functional theory, *Phys. Rev. Lett.*, 1985, **55**, 2471–2474.

122 R. N. Barnett and U. Landman, Born-Oppenheimer molecular-dynamics simulations of finite systems: Structure and dynamcis of $(H_2O)_2$, *Phys. Rev. B: Condens. Matter*, 1993, **48**, 2081–2097.

123 A. Tilocca, Models of structure, dynamics and reactivity of bioglasses: a review, *J. Mater. Chem.*, 2010, **20**, 6848–6858.

124 S. Ispas, M. Benoit, P. Jund and R. Jullien, Structural and electronic properties of the sodium tetrasilicate glass $Na_2Si_4O_9$ from classical and ab initio molecular dynamics simulations, *Phys. Rev. B: Condens. Matter*, 2001, **64**, 214206.

125 D. Donadio, M. Bernasconi and F. Tassone, Photoelasticity of sodium silicate glass from first principles, *Phys. Rev. B: Condens. Matter Mater. Phys.*, 2004, **70**, 214205.

126 A. Tilocca and N. de Leeuw, Structural and electronic properties of modified sodium and soda-lime silicate glasses by Car-Parrinello molecular dynamics, *J. Mater. Chem.*, 2006, **16**, 1950–1955.

127 G. Malavasi, M. C. Menziani, A. Pedone, B. Civalleri, M. Corno and P. Ugliengo, A computational multiscale strategy to the study of amorphous materials, *Theor. Chem. Acc.*, 2007, **117**, 933–942.

128 A. Tilocca and N. H. de Leeuw, Ab-initio molecular dynamics study of 45S5 bioactive silicate glass, *J. Phys. Chem. B*, 2006, **110**, 25810–25816.

129 M. Corno and A. Pedone, Vibrational features of phosphosilicate glasses: Periodic B3LYP simulations, *Chem. Phys. Lett.*, 2009, **476**, 218–222.

130 M. Corno, A. Pedone, R. Dovesi and P. Ugliengo, B3LYP simulation of the full vibrational spectrum of 45S5 bioactive silicate glass compared to v-Silica, *Chem. Mater.*, 2008, **20**, 5610–5621.

131 A. Pedone, T. Charpentier, G. Malavasi and M. C. Menziani, New Insights into the Atomic Structure of 45S5 Bioglass by Means of Solid-State NMR Spectroscopy and Accurate First-Principles Simulations, *Chem. Mater.*, 2010, **22**, 5644–5652.

132 P. E. Blöchl, Projector augmented-wave method, *Phys. Rev. B: Condens. Matter*, 1994, **50**, 17953–17979.

133 P. Pyykkò, Spectroscopic nuclear quadrupole moments, *Mol. Phys.*, 2001, **99**, 1617–1629.

134 A. Soleilhavoup, J.-M. Delaye, F. Angeli, D. Caurant and T. Charpentier, Contribution of first-principles calculations to multinuclear NMR analysis of borosilicate glasses, *Magn. Reson. Chem.*, 2010, **48**, S159–S170.

135 J. P. Perdew, K. Burke and M. Ernzerhof, Generalized Gradient Approximation Made Simple, *Phys. Rev. Lett.*, 1996, **77**, 3865–3868.

136 J. P. Perdew and Y. Wang, Accurate and Simple Analytic Representation of the Electron Gas Correlation Energy, *Phys. Rev. B: Condens. Matter*, 1992, **46**, 6671–6687.

137 L. Truflandier, M. Paris and F. Boucher, DFT investigation of 3d transition metal NMR shielding tensors in diamagnetic systems using the gauge-including projector augmented-wave method, *Phys. Rev. B: Condens. Matter Mater. Phys.*, 2007, **76**, 0703553.

138 M. D. Segall, P. J. D. Lindan, M. J. Probert, C. J. Pickard, P. J. Hasnip, S. J. Clarck and M. C. Payne, First-principles simulation: ideas, illustrations and the CASTEP code, *J. Phys.: Condens. Matter*, 2002, **14**, 2717–2744.

139 P. Giannozzi, S. Baroni, N. Bonini, M. Calandra, R. Car, C. Cavazzoni, D. Ceresoli, G. L. Chiarotti, M. Cococcioni, I. Dabo, A. Dal Corso, S. de Gironcoli, S. Fabris, G. Fratesi, R. Gebauer, U. Gerstmann, C. Gougoussis, A. Kokalj, M. Lazzeri, L. Martin-Samos, N. Marzari, F. Mauri, R. Mazzarello, S. Paolini, A. Pasquarello, L. Paulatto, C. Sbraccia, S. Scandolo, G. Sclauzero, A. P. Seitsonen, A. Smogunov, P. Umari and R. M. Wentzcovitch, QUANTUM ESPRESSO: a modular and open-source software project for quantum simulations of materials, *J. Phys.: Condens. Matter*, 2009, **21**, 395502.

140 A. Sadoc, M. Body, C. Legein, M. Biswal, F. Fayon, X. Rocquefelte and F. Boucher, NMR parameters in alkali, alkaline earth and rare earth fluorides from first principle calculations, *Phys. Chem. Chem. Phys.*, 2011, **13**, 18539–18550.

141 S. Rossano, F. Mauri, C. J. Pickard and I. Farnan, First-Principles Calculation of ^{17}O and ^{25}Mg NMR Shieldings in MgO at Finite Temperature: Rovibrational Effect in Solids, *J. Phys. Chem. B*, 2005, **109**, 7245–7247.

142 I. De Gortari, G. Portella, S. Salvatella, V. S. Bajaj, P. C. A. van der Wel, J. R. Yates, M. D. Segall, C. J. Pickard, M. C. Payne and M. Vendruscolo, Time Averaging of NMR Chemical Shifts in the MLF Peptide in the Solid State, *J. Am. Chem. Soc.*, 2010, **132**, 5993–6000.

143 J.-N. Dumez and C. J. Pickard, Calculation of NMR chemical shifts in organic solids: Accounting for motional effects, *J. Chem. Phys.*, 2009, **130**, 104701–104708.

144 J. Schmidt, J. Hutter, H.-W. Spiess and D. Sebastiani, Beyond Isotropic Tumbling Models: Nuclear Spin Relaxation in Liquids from First Principles, *ChemPhysChem*, 2008, **9**, 2313–2316.

145 T. M. Clark and P. J. Grandinetti, Calculation of bridging ^{17}O quadrupolar coupling parameters on Si–O and Si–O–Si angle, *J. Phys.: Condens. Matter*, 2005, **15**, 2387–2395.

146 T. M. Clark, P. J. Grandinetti, P. Florian and J. F. Stebbins, Correlated structural distributions in silica glass, *Phys. Rev. B: Condens. Matter Mater. Phys.*, 2004, **70**, 064202–064208.

147 F. Mauri, A. Pasquarello, B. G. Pfommer, Y.-G. Yoon and S. G. Louie, Si–O–Si bond-angle distribution in vitreous silica from first-principles ^{29}Si NMR analysis, *Phys. Rev. B: Condens. Matter*, 2000, **62**, 4786–4789.

148 J. Krogh-Moe, The structure of vitreous and liquid boron oxide, *J. Non-Cryst. Solids*, 1969, **1**, 269–284.

149 G. E. J. Jellison, L. W. Panek, P. J. Bray and G. B. J. Rouse, Determinations of structure and bonding in vitreous B_2O_3 by means of ^{10}B, ^{11}B, and ^{17}O NMR, *J. Chem. Phys.*, 1977, **66**, 802–813.

150 S. J. Gravina and P. J. Bray, Nuclear quadrupole resonance of boron in borate glasses, *J. Magn. Reson.*, 1990, **89**, 515–521.

151 C. Joo, U. Werner-Zwanziger and J. W. Zwanziger, The ring structure of boron trioxide glass, *J. Non-Cryst. Solids*, 2000, **261**, 282–286.

152 R. E. Youngman and J. W. Zwanziger, Multiple boron sites in borate glass detected with dynamic angle spinning nuclear magnetic resonance, *J. Non-Cryst. Solids*, 1994, **168**, 293–297.

153 J. A. Tossell, Calculation of the structural and spectral properties of boroxol ring and non-ring B sites in B_2O_3 glass, *J. Non-Cryst. Solids*, 1995, **183**, 307–314.

154 J. W. Zwanziger, The NMR response of boroxol rings: a density functional theory study, *Solid State Nucl. Magn. Reson.*, 2005, **27**, 5–9.

155 J. Swenzon and L. Borjesson, Fraction of boroxol rings in vitreous boron trioxide, *Phys. Rev. B: Condens. Matter*, 1997, **55**, 11138–11143.

156 T. F. Soules, A molecular dynamic calculation of the structure of B_2O_3 glass, *J. Chem. Phys.*, 1980, **73**, 4032–4036.

157 W. Soppe, W. F. van der Marela and H. W. den Hartog, New insights into the structure of B_2O_3 glass, *J. Non-Cryst. Solids*, 1988, **103**, 201–209.

158 P. Umari and A. Pasquarello, Fraction of boroxol rings in vitreous boron oxide from a first-principles analysis of Ramana and NMR spectra, *Phys. Rev. Lett.*, 2005, **95**, 137401.

159 P. Umari and A. Pasquarello, Comment on "fraction of boroxol rings in vitreous boron oxide from first-principles analysis of Raman and NMR spectra"-Umari and Pasquarello reply, *Phys. Rev. Lett.*, 2006, **96**, 199702.

160 M. Kibalchenko, J. R. Yates and A. Pasquarello, First-principles investigation of the relation between structural and NMR parameters in vitreous GeO_2, *J. Phys.: Condens. Matter*, 2010, **22**, 145501–145505.

161 L. S. Du and J. F. Stebbins, Oxygen Sites and Network Coordination in Sodium Germanate Glasses and Crystals: High-Resolution Oxygen-17 and Sodium-23 NMR, *J. Phys. Chem. B*, 2006, **110**, 12427–12437.

162 P. S. Salmon, A. C. Barnes, R. A. Martin and G. J. Cuello, Glass Fragility and Atomic Ordering on the Intermediate and Extended Range, *Phys. Rev. Lett.*, 2006, **96**, 235502.

163 P. S. Salmon, A. C. Barnes, R. A. Martin and G. J. Cuello, Structure of glassy GeO_2, *J. Phys.: Condens. Matter*, 2007, **19**, 415110–415131.

164 L. Giacomazzi, P. Umari and A. Pasquarello, Medium-Range Structural Properties of Vitreous Germania Obtained through First-Principles Analysis of Vibrational Spectra, *Phys. Rev. Lett.*, 2005, **95**, 075505.

165 P. Yang, D. Zhao, D. I. Margolese, B. F. Chmelka and G. D. Stucky, Generalized syntheses of large-pore mesopor-

ous metal oxides with semicrystalline frameworks, *Nature*, 1998, **396**, 152–155.
166 M. J. de Castro, R. Serna, J. A. Chaos, C. N. Afonso and E. R. Hodgson, Influence of defects on the photoluminescence of pulsed-laser deposited Er-doped amorphous Al_2O_3 films, *Nucl. Instrum. Methods Phys. Res., Sect. B*, 2000, **166–167**, 793–797.
167 J. L. Deschanvres, W. Meffre, J. C. Joubert, J. P. Senateur, F. Robaut, J. E. Broquin and R. Rimet, Rare earth-doped alumina thin films deposited by liquid source CVD processes, *J. Alloys Compd.*, 1998, **275–277**, 742–745.
168 S. K. Lee, S. B. Lee, S. Y. Park, Y. S. Yi and C. W. Ahn, Structure of Amorphous Aluminum Oxide, *Phys. Rev. Lett.*, 2009, **103**, 095501.
169 V. Van Hoang and S. K. Oh, Simulation of structural properties and structural transformation of amorphous Al_2O_3, *Phys. B*, 2004, **352**, 73–85.
170 R. Lizárraga, E. Holmström, S. C. Parker and C. Arrouvel, Structural characterization of amorphous alumina and its polymorphs from first-principles XPS and NMR calculations, *Phys. Rev. B: Condens. Matter Mater. Phys.*, 2011, **83**, 094201.
171 E. Schneider, J. F. Stebbins and A. Pines, Speciation and local structure in alkali and alkaline earth silicateglasses constraints from ^{29}Si NMR spectroscopy, *J. Non-Cryst. Solids*, 1987, **89**, 371–383.
172 K. E. Kelsey, J. R. Allwart and J. F. Stebbins, Ca–Mg mixing in aluminosilicate glasses: An investigation using ^{17}O MAS and 3QMAS and ^{27}Al MAS NMR, *J. Non-Cryst. Solids*, 2008, **354**, 4644–4653.
173 J. R. Allwardt, S. K. Lee and J. F. Stebbins, Bonding preferences of non-bridging oxygens in calcium aluminosilicate glass: evidence from ^{17}O MAS and 3QMAS NMR on calcium aluminate and low-silica ca-aluminosilicate glasses, *Am. Mineral.*, 2003, **88**, 949–954.
174 F. Angeli, O. Villain, S. Schuller, S. Ispas and T. Charpentier, Insight into sodium silicate glass structural organization by multinuclear NMR combined with first-principles calculations, *Geochim. Cosmochim. Acta*, 2011, **75**, 2453–2469.
175 S. Ispas, T. Charpentier, F. Mauri and D. R. Neuville, Structural properties of lithium and sodium tetrasilicate glasses: Molecular dynamics simulations versus NMR experimental and first-principles data, *Solid State Sci.*, 2010, **12**, 183–192.
176 P. Zhang, P. J. Grandinetti and J. F. Stebbins, Anoinic Species Determination in $CaSiO_3$ Glass Using Two-Dimensional ^{29}Si NMR, *J. Phys. Chem. B*, 1997, **101**, 4004–4008.
177 R. N. Mead and G. Mountjoy, A molecular dynamics study of the atomic structure of $(CaO)_x(SiO_2)_{1-x}$ glasses, *J. Phys. Chem. B*, 2006, **110**, 14273–14278.
178 S. Sen and J. Tangeman, Evidence for anomalously large degree of polymerization in Mg_2SiO_4 glass and melt, *Am. Mineral.*, 2008, **93**, 946–949.
179 R. Radeglia and G. Engelhardt, Correlation of Si–O–T (T = Si or Al)-angles and ^{29}Si NMR chemical shifts in silicate and aluminosilicates, *Chem. Phys. Lett.*, 1985, **114**, 28–30.
180 R. F. Pettifer, E. Dupree, I. Farnan and U. Stenberg, NMR determinations of Si–O–Si bond angle distributions in silica, *J. Non-Cryst. Solids*, 1988, **106**, 408–412.
181 J. F. Gladden, T. A. Carpenter and S. R. Elliot, ^{29}Si MAS NMR studies of the spin lattice relaxation time and bond angle distribution in vitreous silica, *Philos. Mag. B*, 1986, **53**, 81–87.
182 L. M. Bull, B. Bussemer, T. Anupold, A. Reinhold, S. A. J. Sauer, A. K. Cheetham and R. Dupree, A high-resolution ^{17}O and ^{29}Si NMR study of zeolite siliceous ferrierite and ab initio calculations of NMR parameters, *J. Am. Chem. Soc.*, 2000, **122**, 4948–4958.
183 P. Florian, F. Fayon and D. Massiot, ^{2}J Si–O–Si Scalar Spin–Spin Coupling in the Solid State: Crystalline and Glassy Wollastonite $CaSiO_3$, *J. Phys. Chem. C*, 2009, **113**, 2562–2572.
184 R. Mozzi and B. E. Warren, The structure of vitreous silica, *J. Appl. Crystallogr.*, 1969, **2**, 164–172.
185 H. F. Poulsen, J. Neuefeind, H. B. Neumann, J. R. Schneider and M. D. Zeidler, Amorphous silica studied by high-energy X-ray diffraction, *J. Non-Cryst. Solids*, 1995, **188**, 63–74.
186 J. R. G. de Silva, D. G. Pinatti, C. E. Anderson and M. L. Rudee, Refinement of structure of vitreous silica, *Philos. Mag.*, 1975, **31**, 713–717.
187 C. Gervais, D. Laurencin, A. Wong, F. Pourpoint, J. Labram, B. Woodward, A. P. Howes, K. J. Pike, R. Dupree, F. Mauri, C. Bonhomme and M. E. Smith, New perspectives on calcium environments in inorganic materials containing calcium-oxygen bonds: A combined computational-experimental ^{43}Ca NMR approach, *Chem. Phys. Lett.*, 2008, **464**, 42–48.
188 F. Angeli, M. Gaillard, P. Jollivet and T. Charpentier, Contribution of ^{43}Ca MAS NMR for probing the structural configuration of calcium in glass, *Chem. Phys. Lett.*, 2007, **440**, 324–328.
189 K. Shimoda, Y. Tobu, Y. Shimoikeda, T. Nemoto and K. Saito, Multiple Ca^{2+} environments in silicate glasses by high-resolution ^{43}Ca MQMAS NMR technique at high and ultra-high (21.8 T) magnetic fields, *J. Magn. Reson.*, 2007, **186**, 156–159.
190 D. Laurencin and M. E. Smith, Development of ^{43}Ca solid state NMR spectroscopy as a probe of local structure in inorganic and molecular materials, *Prog. Nucl. Mag. Res. Spectrosc.*, 2012.
191 E. Muller, K. Heide and E. D. Zanotto, Molecular structure and nucleation in silicate glasses, *J. Non-Cryst. Solids*, 1993, **155**, 56–66.
192 M. J. Toplis, D. B. Dingwell and T. Lenci, Peraluminous Viscosity Maxima in Na_2O–Al_2O_3–SiO_2 Liquids: The Role of Triclusters in Tectosilicate Melts, *Geochim. Cosmochim. Acta*, 1997, **61**, 2605–2612.
193 J. F. Stebbins and Z. Xu, NMR evidence for excess non-bridging oxygen in an aluminosilicate glass, *Nature*, 1997, **390**, 60–62.
194 M. Benoit, M. Profeta, F. Mauri, C. J. Pickard and M. E. Tuckerman, First-Principles Calculations of the ^{17}O NMR Parameters of a Calcium aluminosilicate Glass, *J. Phys. Chem. B*, 2005, **109**, 6052–6060.
195 S. K. Lee and J. F. Stebbins, The Structure of Aluminosilicate Glasses: High-Resolution ^{17}O and ^{27}Al MAS and 3QMAS NMR Study, *J. Phys. Chem. B*, 2000, **104**, 4091–4100.

196 S. K. Lee and J. F. Stebbins, The distribution of sodium ions in aluminosilicate glasses: a high field ^{23}Na MAS and 3QMAS NMR study, *Geochim. Cosmochim. Acta*, 2003, **67**, 1699–1709.

197 J. A. Tossell, in *Molecular modelling theory: applications in the Geosciences*, eds. R. T. Cygan and J. D. Kubicki, Mineralogical Soc. Amer., Chantilly, VA, USA, 2001, vol. 42, pp. 437–458.

198 Y. Liu, H. Nekvasil and J. A. Tossell, Explaining the Effects of T–O–T Bond Angles on NMR Chemical Shift in Aluminosilicates: A Natural Bonding Orbital (NBO) and Natural Chemical Shielding (NCS) Analysis, *J. Phys. Chem. A*, 2005, **109**, 3060–3066.

199 L. L. Hench, R. J. Splinter, W.-C. Allen and T. Greenle, Bonding mechanisms at the interface of ceramic prosthetic materials, *J. Biomed. Mater. Res.*, 1971, **2**, 117–141.

200 I. D. Xynos, A. J. Edgar, L. D. Buttery, L. L. Hench and J. M. Polak, Gene-expression profiling of human osteoblasts following treatment with ionic products of Bioglass 45S5 dissolution, *J. Biomed. Mater. Res.*, 2001, **55**, 151–157.

201 V. FitzGerald, D. M. Pickup, H. D. C. Greenspan, G. Sarkar, J. J. Fitzgerald, K. M. Wetherall, R. B. Moss, J. R. Jones and R. J. Newport, A Neutron and X-Ray Diffraction Study of Bioglas® with Reverse Monte. Carlo Modelling, *Adv. Funct. Mater.*, 2007, **17**, 3746–3753.

202 I. Elgayar, A. E. Aliev, A. R. Bocaccini and R. G. Hill, Structural Analysis of Bioactive Glasses, *J. Non-Cryst. Solids*, 2005, **351**, 173–183.

203 D. S. Brauer, N. Karpukhina, R. V. Law and R. G. Hill, Structure of fluoride-containing bioactive glasses, *J. Mater. Chem.*, 2009, **19**, 5629–5636.

204 M. W. G. Lockyer, D. Holland and R. Dupree, NMR investigation of the structure of some bioactive and related glasses, *J. Non-Cryst. Solids*, 1995, **188**, 207–219.

205 A. Angelopoulou, V. Montouillout, D. Massiot and G. Kordas, Study of the alkaline environment in mixed alkali compositions by multiple-quantum magic angle nuclear magnetic resonance (MQMAS NMR), *J. Non-Cryst. Solids*, 2008, **354**, 333–340.

206 C. C. Lin, L. C. Huang and P. Shen, $Na_2CaSi_2O_6$–P_2O_5 based bioactive glasses. Part 1:Elasticity and structure, *J. Non-Cryst. Solids*, 2005, **351**, 3195–3203.

207 A. Tilocca, Structure and dynamics of bioactive phosphosilicate glasses and melts from ab initio molecular dynamics simulations, *Phys. Rev. B: Condens. Matter Mater. Phys.*, 2007, **76**, 224202–224213.

208 A. Tilocca, A. N. Cormack and N. de Leeuw, The structure of bioactive silicate glasses: New insight from molecular dynamics simulations, *Chem. Mater.*, 2007, **19**, 95.

209 J. M. Oliveira, R. N. Correia and M. H. Fernandes, Effects of Si speciation on the in vitro bioactivity of glasses, *Biomaterials*, 2002, **23**, 371–379.

210 H. A. Elbatal, M. A. Azooz, E. M. A. Khalil, A. Soltan Monem and Y. M. Hamdy, Characterization of some bioglass-ceramics, *Mater. Chem. Phys.*, 2003, **80**, 599–609.

211 C. Bonhomme, C. Gervais, N. Folliet, F. Pourpoint, C. C. Diogo, J. Lao, E. Jallot, J. Lacroix, J. M. Nedelec, D. Iuga, J. V. Hanna, M. E. Smith, Y. Xiang, J. Du and D. Laurencin, ^{87}Sr Solid-State NMR as a Structurally Sensitive Tool for the Investigation of Materials: Antiosteoporotic Pharmaceuticals and Bioactive Glasses, *J. Am. Chem. Soc.*, 2012, **134**, 12611–12628.

212 B. H. DeJong, C. M. Schramm and V. E. Parziale, ^{29}Si magic angle spinning NMR on local silicon environments in amorphous and crystalline lithium silicates, *J. Am. Chem. Soc.*, 1984, **106**, 4396–4402.

213 P. Zhang, P. J. Grandinetti and J. F. Stebbins, Anionic Species Determination in $CaSiO_3$ Glass using Two-dimensional ^{29}Si NMR, *J. Phys. Chem. B*, 1997, **101**, 4004–4008.

214 G. Lusvardi, G. Malavasi, M. Cortada, L. Menabue, M. C. Menziani, A. Pedone and U. Segre, Elucidation of the Structural role of Fluorine Potential Bioactive Glasses by Experimental and Computational Investigation, *J. Phys. Chem. B*, 2008, **112**, 12730–12739.

215 M. Veshtort and R. G. Griffin, SPINEVOLUTION: A powerful tool for the simulation of solid state and liquid state NMR experiments, *J. Magn. Reson.*, 2006, **178**, 248–282.

216 J. Isaac, J. Nohra, J. Lao, E. Jallot, J. M. Nedelec, A. Berdal and J. M. Sautier, Effects of strontium-doped bioactive glass on the differentiation of cultured osteogenic cells, *Eur. Cells Mater.*, 2011, **21**, 130–143.

217 J. Lao, J. M. Nedelec and E. Jallot, New strontium-based bioactive glasses: physicochemical reactivity and delivering capability of biologically active dissolution products, *J. Mater. Chem.*, 2009, **19**, 2940–2949.

218 M. J. Plodinec, Borosilicate glasses for nuclear waste imobilisation, *Glass Technol.*, 2000, **41**, 186–192.

219 A. Quintas, D. Caurant, O. Majérus, T. Charpentier and J.-L. Dussossoy, Effect of compositional variations on charge compensation of AlO_4 and BO_4 entities and on crytsallization tendency of a rare-earth-rich aluminoborosilicate glass, *Mater. Res. Bull.*, 2009, **44**, 1895–1898.

220 T. Advocat, P. Jollivet, J. L. Crovisier and M. D. Nero, Long-term alteration mechanisms in water for SON68 radioactive borosilicate glass, *J. Nucl. Mater.*, 2001, **298**, 55–62.

221 T. W. T. Tsai, Y. Mou, Y.-H. Tseng, L. Zhang and J.-L. Dussossoy, Solid-State NMR Study of Bioactive Binary Borosilicate Glasses, *J. Phys. Chem. Solids*, 2008, **69**, 2628–2633.

222 S. Wang and J. F. Stebbins, Multiple-quantum magic-angle spinning ^{17}O NMR studies of borate, borosilicate and boroaluminate glasses, *J. Am. Ceram. Soc.*, 1999, **82**, 1680–1684.

223 R. Martens and W. Müller-Warmuth, Structural groups and their mixing in borosilicate glasses of various compositions-an NMR study, *J. Non-Cryst. Solids*, 2000, **265**, 167–175.

224 S. K. Lee, C. B. Musgrave, P. Zhao and J. F. Stebbins, Topological disorder and reactivity of borosilicate glasses: quantum chemical calculations and ^{17}O and ^{11}B NMR study, *J. Phys. Chem. B*, 2001, **105**, 12583–12595.

225 L. van Wüllen and G. Schwering, ^{11}B-MQMAS and ^{29}Si-{^{11}B} double resonance NMR studies on the structure of binary B_2O_3–SiO_2 glasses, *Solid State Nucl. Magn. Reson.*, 2002, **21**, 134–144.

226 I. Hung, A. P. Howes, B. G. Parkinson, T. Anupold, A. Samoson, S. P. Brown, P. F. Harrison, D. Holland and R. Dupree, Determination of the bond-angle distribution

in vitreous B_2O_3 by ^{11}B double rotation (DOR) NMR spectroscopy, *J. Solid State Chem.*, 2009, **182**, 2402–2408.
227 F. Angeli, O. Villain, S. Schuller, T. Charpentier, D. de Ligny, L. Bressel and L. Wondraczek, Effect of temperature and thermal history on borosilicate glass structure, *Phys. Rev. B: Condens. Matter Mater. Phys.*, 2012, **85**, 054110.
228 F. Fayon, I. J. King, R. K. Harris, J. S. O. Evans and D. Massiot, Application of the through-bond correlation NMR experiment to the characterization of crystalline and disordered phosphates, *C. R. Chim.*, 2004, **7**, 351–361.
229 J. V. Hanna and M. E. Smith, Recent technique developments and applications of solid state NMR in characterising inorganic materials, *Solid State Nucl. Magn. Reson.*, 2010, **38**, 1–18.
230 G. Tricot, L. Delevoye, G. Palavit and L. Montagne, Phase identification and quantification in a devitrified glass using homo- and heteronuclear solid-state NMR, *Chem. Commun.*, 2005(42), 5289–5291.
231 B. Raguenet, G. Tricot, G. R. Silly and M. A. Pradel, Revisiting the 'mixed glass former effect' in ultra-fast quenched borophosphate glasses by advanced 1D/2D solid state NMR, *J. Mater. Chem.*, 2011, **21**, 17693–17704.
232 B. Chen, U. Werner-Zwanziger, M. L. F. Nasciemento, L. Ghussn, E. D. Zanotto and J. W. Zwanziger, Structural Similarity on Multiple Length Scales and its Relation to Devitrification Mechanims: A Soldi-State NMR Study of Alkali Diborate Glasses and Crystals, *J. Phys. Chem. C*, 2009, **113**, 20725–20732.
233 T. Vosegaard, Challenges in numerical simulations of solid-state NMR experiments: spin exchange pulse sequences, *Solid State Nucl. Magn. Reson.*, 2010, **38**, 77–83.
234 P. Hodgkinson and L. Emsley, Numerical simulation of soldi-state NMR experiments, *Prog. Nucl. Magn. Reson. Spectrosc.*, 2000, **36**, 201–239.
235 P. Cimino, A. Pedone, E. Stendardo and V. Barone, Interplay of stereo-electronic, environmental, and dynamical effects in determining the EPR parameters of aromatic spin-probes: INDCO as a test case, *Phys. Chem. Chem. Phys.*, 2010, **12**, 3741–3746.
236 V. Barone, P. Cimino and A. Pedone, An integrated computational protocol for the accurate prediction of EPR and PNMR parameters of aminoxyl radicals in solution, *Magn. Reson. Chem.*, 2010, **48**, S11–S22.
237 E. Stendardo, A. Pedone, P. Cimino, M. C. Menziani, M. Crescenzi and V. Barone, Extension of the AMBER force-field for the study of large nitroxides in condensed phases: an ab initio parameterization, *Phys. Chem. Chem. Phys.*, 2010, **12**, 11697–11709.
238 J. T. Nielsen, H. R. Eghbalnia and N. C. Nielsen, Chemical shift prediction for protein structure calculation and quality assessment using an optimally parameterized force field, *Prog. Nucl. Magn. Reson. Spectrosc.*, 2012, **60**, 1–28.
239 S. K. Lee and J. F. Stebbins, Disorder and the extent of polymerization in calcium silicate and aluminosilicate glasses: ^{17}O NMR results and quantum chemical molecular orbital calculations, *Geochim. Cosmochim. Acta*, 2006, **70**, 4275.

